JCIM JOURNAL OF CHEMICAL INFORMATION AND MODELING

pubs.acs.org/jcim Article

Structural Determinants of Buprenorphine Partial Agonism at the μ-Opioid Receptor

Antoniel A. S. Gomes and Jesús Giraldo*

Cite This: J. Chem. Inf. Model. 2025, 65, 5071−5085 Read Online

ABSTRACT: The μ-opioid receptor (μOR) is a class A G Protein-Coupled Receptor (GPCR) targeted by natural and synthetic ligands to provide analgesia to patients with pain of various etiologies. Available opioid medications present several unwanted side effects, stressing the need for safer pain therapies. Despite the attractive proposal that biasing μOR signaling toward G protein pathways would lead to fewer side effects, recent studies indicate that low-efficacy opioid drugs, such as buprenorphine, may represent a safer alternative. In the present work, we combine molecular docking, microsecond-time scale molecular dynamics (MD) simulations, and metadynamics to investigate the conformational dynamics of the μOR bound to morphine or buprenorphine. Our objective was to determine structural aspects associated with the unique pharmacological effects caused by the latter, taking morphine as a reference. MD simulations identified a salt bridge with D149$^{3.32}$ as crucial for stabilizing both ligands into the μOR orthosteric site, with this interaction being weaker in buprenorphine. The morphinan-scaffold of both ligands shared contacts with transmembrane (TM) helix residues of the receptor, including TM3, TM5, TM6, and TM7. Conversely, while morphine showed stronger interactions with a few TM3 residues, additional chemical groups of buprenorphine showed stronger interactions with TM2, extracellular loop 2 (ECL2), and TM7 residues. We also observed distinct TM arrangements induced by these ligands, with buprenorphine causing an extracellular outward movement of TM7 and morphine provoking intracellular inward movements of TM5 and TM7 of the receptor. In addition, we found that buprenorphine tends to explore deeper regions in the μOR orthosteric site, further supported by funnel-metadynamics, resulting in diverse side chain orientations of W295$^{6.48}$. Metadynamics also unveiled distinct intermediate states for morphine and buprenorphine, with the latter accessing a secondary binding site associated with partial μOR agonists. Our results indicate that the weakened salt bridge of buprenorphine with D149$^{3.32}$, along with the strong TM7 interaction through its cyclopropyl group, may explain its low efficacy and consequent partial μOR agonism. Furthermore, ECL2 interactions may contribute to explaining the biased agonism of buprenorphine, a common feature shared with other opioid modulators with similar functional effects. Our study sheds light on the complex pharmacology of buprenorphine, identifying structural aspects associated with its partial and biased μOR agonism. These results can provide valuable information for the design of new effective and safer opioid drugs.

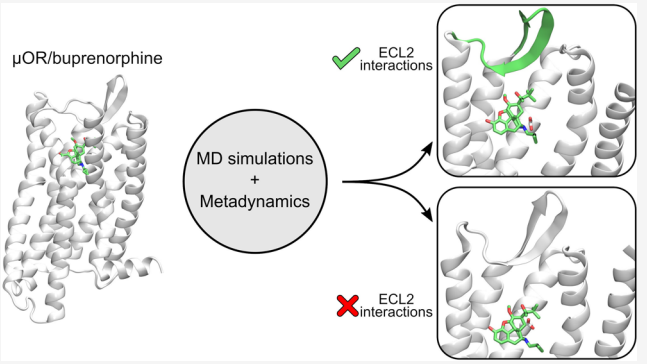

INTRODUCTION

Chronic pain is a major public health problem that, according to studies and regions, affects between 20 and 30% of the population.[1,2] Opioid-mediated analgesia remains the most effective treatment for severe acute and cancer pain; however, it is not so effective for chronic pain, where the severe side effects that opioids may exert, including addiction, nausea, constipation, and respiratory depression, make their long-term use not recommended.[3] Importantly, the abuse of opioids can lead to overdose and consequent respiratory depression, which may have fatal consequences, resulting in the so-called "opioid crisis".[4] Remarkably, nearly 108,000 persons in the U.S. died from drug-involved overdose in 2022, including from illicit or prescription drugs, of which nearly 74,000 involved synthetic opioids other than methadone, primarily fentanyl.[5] Furthermore, the number of overdose deaths caused by opioids has increased alarmingly 5-fold in the past decade, indicating that it is not a one-time, stabilized problem.[6] Therefore, the development of effective therapeutic strategies with fewer secondary effects is essential in pain treatment.

Opioids target a family of G Protein-Coupled Receptors (GPCRs), known as opioid receptors (ORs). These receptors include mu (μOR), delta (δOR), kappa (κOR), and nociception receptor (NOP), with μOR considered the most

Received: January 17, 2025
Revised: April 2, 2025
Accepted: April 9, 2025
Published: May 6, 2025

https://doi.org/10.1021/acs.jcim.5c00078
J. Chem. Inf. Model. 2025, 65, 5071−5085

relevant receptor to promote analgesia.[7] The classification of μOR, δOR, and κOR is based on their distinct pharmacology,[8] developmental expression,[9] and brain distribution.[10] Later, NOP was included due to its responsiveness to morphine-like ligands and opioid peptides.[11] As GPCRs, the signaling of ORs involves various intracellular proteins, including G proteins, GPCR kinases (GRKs), and β-arrestins.[12] Activation of ORs primarily leads to G protein coupling, preferentially to the Gi/o family, a heterotrimer consisting of Gα, Gβ, and Gγ subunits. While Gα inhibits cAMP production, Gβ and Gγ regulate ion channels, preventing calcium influx and potassium efflux from cells and inhibiting vesicle SNAP receptors (SNAREs). This results in neuronal hyperpolarization and reduces the presynaptic release of neurotransmitters, thereby attenuating pain signaling and providing analgesia.[13] Desensitization of OR signaling is reached when the receptor is phosphorylated by GRKs, which increases its affinity to β-arrestin, leading to receptor internalization via membrane-associated clathrins endocytosis.[12] β-arrestin also modulates several kinases signaling pathways, such as extracellular signal-regulated kinases (ERKs), Jun N-terminal kinases (JNKs), and mitogen-activated protein kinases (MAPKs).[13]

Pioneering works showed that morphine can enhance and prolong analgesia in mice lacking β-arrestin 2, likely due to μOR desensitization impairment.[14,15] Further, β-arrestin 2 knockout in mice was associated with reduced morphine respiratory suppression and acute constipation.[16] These findings provided compelling evidence to discriminate pharmacological aspects of μOR, indicating that β-arrestin signaling contributes to opioid secondary side effects while G protein-biased signaling could expand the therapeutic window for developing safer treatments for chronic pain.[17] This finding guided the search and development of new opioid modulators that exhibit weak β-arrestin recruitment, aiming to reduce side effects. This effort led to the discovery of compounds such as oliceridine (TRV130),[18] PZM21,[19] SR-17018,[17] FH210,[20] and mitragynine-pseudoindoxyl (MP).[21] However, further findings suggested that morphine-induced respiratory depression might be attributed to neuron hyperpolarization through μOR activation,[22] such as the modulation of G protein-gated inwardly rectifying potassium (GIRK) channels.[23] Moreover, a study with phosphorylation-deficient μORs showed improved analgesia and reduced tolerance while either preserving or worsening the secondary effects of morphine and fentanyl.[24] Furthermore, the same team found that morphine-induced respiratory depression in knockout mice was independent of β-arrestin 2 signaling, questioning the efforts for developing opioid modulators biased toward G protein signaling.[25]

Further studies have reclassified TRV130 and PZM21 as G protein partial agonists at the μOR.[26] These insights have led to the formulation of an alternative proposal suggesting that the low intrinsic efficacy of opioid ligands at the μOR is associated with diminished side effects,[27] thus providing new potential alternatives for improved therapeutic windows in chronic pain treatment. As a result, TRV130 became the first biased agonist approved by the FDA for treating moderate to severe acute pain in adults.[28] It also extends to other biased agonists that are also partial agonists, such as SR-17018,[17] FH210,[20] and MP,[21] suggesting a relationship between their functional properties and safer effect profiles with weak agonism.[29,30] In addition, recent findings indicate that opioid ligands with high intrinsic efficacy toward G protein signaling are associated with increased risk of intoxication and overdose.[31] These results open new paths toward more efficient therapeutics of partial agonists to provide analgesia.[32,33] Among these, buprenorphine is considered a partial agonist at the μOR, widely used in chronic pain management due to its ceiling effect on sedation and respiratory depression.[34] Buprenorphine has a notable application in patients with substance dependence and opioid abuse[35−37] due to its rewarding effects[38] and its ability to compete with substances such as heroin.[39] Despite being a partial agonist, buprenorphine provides analgesia equivalent to full agonists, with its specific role at spinal instead of brain opioid receptors potentially accounting for its reduced secondary effects.[40] Given its lower abuse potential and enhanced safety, buprenorphine is recommended for pain management in perioperative patients.[41] Interestingly, buprenorphine is also identified as a biased agonist favoring G protein signaling,[31,42,43] underscoring its importance in functional and structural studies of μOR modulation.[42−44]

The understanding of μOR functional aspects from a structural perspective started with elucidating the crystallographic structure of the μOR from mice,[45] revealing its orthosteric site. Subsequent efforts determined the active, inactive, and intermediate conformations of the μOR when bound to various opioid modulators.[13] Recently, a highly relevant work revealed the structural determinants of the μOR/morphine complex by cryo-electron microscopy (cryo-EM),[46] validating the ligand orientation typically observed in morphinan-scaffold ligands interacting with μOR.[44,45,47,48] Advances in experimental conformational dynamics of the μOR have demonstrated that ligands alone can induce notably conformational changes in intracellular loop 1 (ICL1) and helix 8 (H8), with notable changes in transmembrane helices 5 and 6 (TM5 and TM6) observed only in the presence of G protein.[49] Further, Cong et al. suggested that these conformational changes can discriminate between biased and unbiased μOR agonists.[43]

Together with experimental works, computational studies have substantially advanced the structural understanding of the μOR, identifying key residues for ligand binding,[20,44,46,50−53] determining local and global conformational changes induced by ligands,[21,54−57] exploring intermediate ligand states,[58,59] explaining ligand functional selectivity,[60] and reproducing experimental kinetics properties, such as ligand residence time[61] and binding affinity.[62] These efforts have been essential for relating structural and functional aspects of the μOR, allowing the development of an initial model that explains how distinct ligand−receptor interactions result in biased signaling at the μOR.[51] However, subsequent research indicated that this model does not account for the biased behavior of PZM21.[20] Indeed, none of these models include morphinan-scaffold ligands, such as buprenorphine, reinforcing the need for further investigations to improve the understanding of the structure and function relationship in μOR signaling.

To date, the experimental structure of the μOR/buprenorphine complex is still unknown, although some computational studies have investigated its interaction with the μOR. Classical Molecular Dynamics (MD) simulations have indicated that buprenorphine induces a specific outward movement of the extracellular side of TM7 in the μOR, which is prevented by the presence of a positive allosteric modulator, forcing buprenorphine to behave similarly to full agonists.[54] Moreover, classical and accelerated MD simulations have shown that buprenorphine interacts with a higher number of

https://doi.org/10.1021/acs.jcim.5c00078
J. Chem. Inf. Model. 2025, 65, 5071−5085

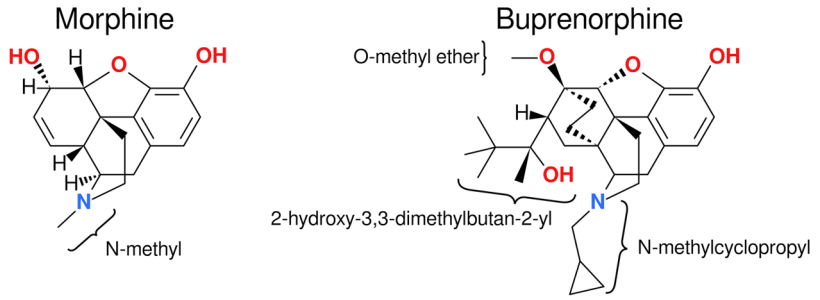

Figure 1. 2D representation of morphine and buprenorphine. Morphine and buprenorphine chemical groups are indicated. Oxygen and nitrogen atoms are colored red and blue, respectively.

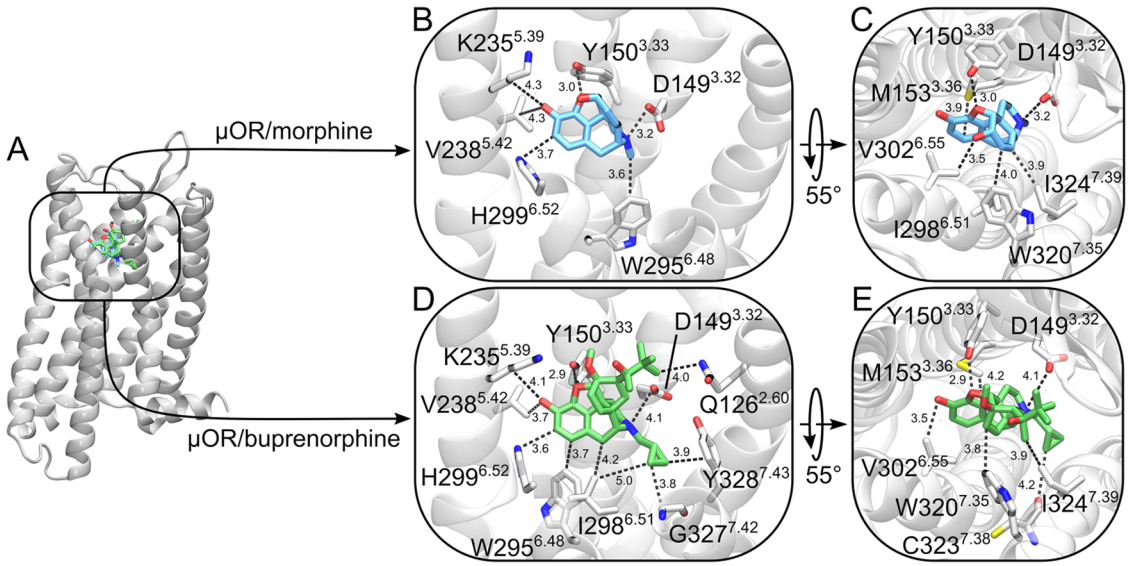

Figure 2. Representative conformations of the μOR/morphine and μOR/buprenorphine complexes obtained from MD simulations. (A) Both ligands are stabilized at the μOR orthosteric site, and (B–E) exhibit similar residue interactions with the receptor. Morphine and buprenorphine are represented as cyan and green sticks, respectively, while the μOR is depicted as silver cartoons. μOR residues in contact with each ligand within 5 Å are presented as sticks. For a cleaner visualization, μOR residues from I300$^{6.53}$ to A325$^{7.40}$ were removed.

residues compared to norbuprenorphine (a metabolite of buprenorphine) or diprenorphine, potentially contributing to its slower dissociation rate.[50] The slow dissociation rate of buprenorphine was further predicted by infrequent metadynamics, which also described the dissociation pathway of this ligand, revealing distinct intermediate binding sites.[61] Moreover, replica exchange with solute tempering (REST2) MD simulations has suggested that the partial agonism effect of buprenorphine might derive from its inability to stabilize the tryptophan residue (W295$^{6.48}$) located deep in the μOR orthosteric site.[43] Although these studies present preliminary efforts to explain the functional effects of buprenorphine at the μOR, a comprehensive understanding of the structural aspects of its complex partial and biased agonism requires further investigation. Here, we used molecular docking followed by long-time scale MD simulations to identify critical μOR residues that stabilize buprenorphine and search for local and global conformational changes in the receptor induced by this ligand. In addition, we applied the funnel-metadynamics technique[62] to estimate the binding affinity and identify intermediate states of buprenorphine. To check the validity of our results, we used the same protocol for morphine, a μOR agonist. Our comparative results show a detailed conformational description that offers novel insights into μOR partial agonism. These results may complement previous models,[20,51] thus providing a more complete description of the partial and biased agonism of μOR. Because the differential functional effects of ligands on a particular receptor depend on their structure, Figure 1 depicts the two-dimensional (2D) structure of morphine and buprenorphine as a reference image for the ligand–receptor interactions described in the results section.

RESULTS

In this study, we mainly focused on determining the structural effects induced by morphine and buprenorphine on the μOR starting from the inactive conformation of the receptor (conformational induction), employing classical MD simulations and funnel-metadynamics techniques. Additionally, we performed classical MD simulations of the μOR bound to these ligands, starting from the active conformation as a complementary (conformational selection) approach (refer to Supporting Information). Table S1 provides a detailed overview of the simulation conditions for all systems. To facilitate comparison with other receptors, we used Ballesteros–Weinstein numbering as superscript.[63]

Predicting the Binding of Buprenorphine to the μOR Orthosteric Site. We performed molecular docking to obtain an initial orientation of buprenorphine into the μOR orthosteric site using AutoDock-GPU.[64] We used the human

https://doi.org/10.1021/acs.jcim.5c00078
J. Chem. Inf. Model. 2025, 65, 5071–5085

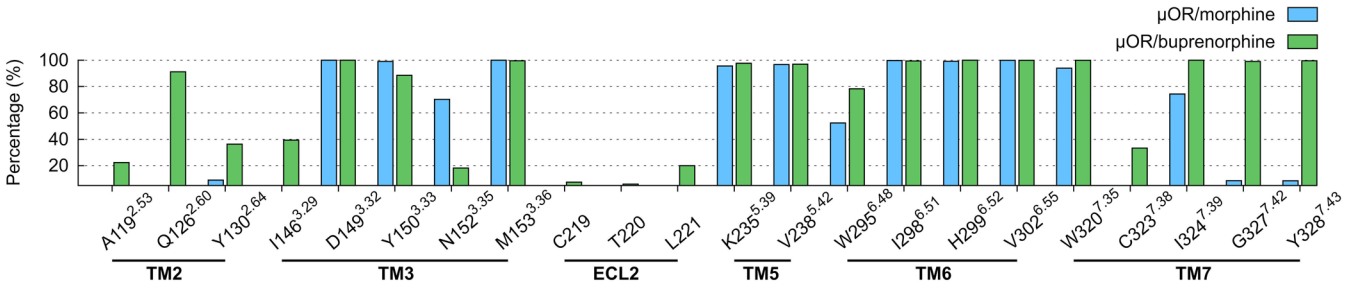

Figure 3. Percentage of contacts of μOR residues with morphine and buprenorphine during MD simulations. μOR residues in contact with morphine and buprenorphine are depicted as cyan and green bars, respectively.

inactive μOR structure, modeled from mouse (PDB code 7UL4).[65] The same protocol was applied to morphine. The poses with the lowest estimated free energy of binding (Δ*G*) for buprenorphine and morphine were −9.94 and −7.51 kcal/mol, respectively. Recent work revealed the μOR/morphine structure by cryo-EM, highlighting the classical salt bridge between the carboxylate group of D149$^{3.32}$ and the protonated amine group of the ligand, together with the interaction of the hydroxyl group of Y150$^{3.33}$ with the oxygen of the partially saturated furan ring of morphine.[46] We observed a similar orientation for both molecules, with morphine presenting a root-mean-square deviation (RMSD) of 1.39 Å for non-hydrogen atoms after superposing the receptor backbone atoms (Figure S1A,B). Conversely, buprenorphine presented a slight rotation, leading to an interaction of its *O*-methyl ether and hydroxyl groups with Y150$^{3.33}$ (Figure S1C).

We submitted each complex to MD simulations to investigate their dynamic behavior and obtain a stable conformation for the ligands at the μOR orthosteric site. Data from 4 independent replicas for each complex were analyzed. Both morphine and buprenorphine presented high stability at the μOR orthosteric site, as evidenced by stable RMSD calculation of non-hydrogen atoms, with average values of 1.86 (0.49 SD) and 2.6 (0.63 SD) Å, respectively (Figure S2). We calculated the average structure of each complex for each replica to obtain the final stabilized orientation of buprenorphine and morphine at the μOR orthosteric site. Representative structures were obtained by selecting the frame with the lowest all-atom RMSD relative to the average structure to illustrate the orientation of each molecule, highlighting critical μOR residues for stabilizing the complex (Figure 2).

Following MD simulations, buprenorphine was accommodated into the μOR orthosteric site (Figure 2A), maintaining the salt bridge between its amine group and the carboxylate of D149$^{3.32}$ of the receptor and stabilizing its furan-ring oxygen with the hydroxyl group of Y150$^{3.33}$, assuming a morphine-like orientation (Figure 2B−E). Given the common morphinan-scaffold, several μOR residues of TM3 and TM5−7, such as M153$^{3.36}$, K235$^{5.39}$, V238$^{5.42}$, W295$^{6.48}$, I298$^{6.51}$, H299$^{6.52}$, V302$^{6.55}$, W320$^{7.35}$, and I324$^{7.39}$, are common to both ligands. Buprenorphine's additional chemical groups resulted in particular interactions, as observed by its 2-hydroxy-3,3-dimethylbutan-2-yl group engaging TM2 (Q126$^{2.60}$) interactions and its *N*-methylcyclopropyl group interacting with TM7 residues deep within the μOR orthosteric site, such as C323$^{7.38}$, G327$^{7.42}$, and Y328$^{7.43}$. Interestingly, the average structure of both ligands was similar across all replicas, indicating convergence to a favorable and stable conformation (Figure S3). Therefore, we assume that these average conformations likely represent stable orientations of each ligand at the μOR orthosteric site.

Buprenorphine Presents Distinct μOR Residue Interactions. After exploring the average structure of both ligands, we analyzed the involvement of μOR residues in ligand stabilization from a dynamic perspective. To this end, we calculated the percentage of contacts with each μOR residue within a 4 Å cutoff (Figure 3). We confirmed that both ligands frequently interact with D149$^{3.32}$ during the simulation time. Additionally, we identified other residues that stabilized both ligands for more than 95% of the time, mainly located in TM5 and TM6, such as K235$^{5.39}$, V238$^{5.42}$, I298$^{6.51}$, H299$^{6.52}$, and V302$^{6.55}$, including the TM3 residue M153$^{3.36}$, with over 99% contact time. These residues, surrounding the morphinan-scaffold of both ligands, likely contribute to stabilizing buprenorphine and morphine. We also observed the role of Y150$^{3.33}$ in stabilizing both molecules despite the reduced interaction with buprenorphine (88.5%) compared to morphine (99%).

To determine residues distinctly interacting with buprenorphine or morphine, we selected those exhibiting differences between the complexes greater than 5%. Buprenorphine's additional chemical groups facilitated exclusive interactions with TM2 and TM7 residues (Figure 2B−C). Thus, buprenorphine's cyclopropyl group strongly interacted with TM7 residues (>90%), such as W320$^{7.35}$, I324$^{7.39}$, G327$^{7.42}$, and Y328$^{7.43}$. Except for W320$^{7.35}$ and I324$^{7.39}$, these residues showed minimal interaction with morphine (<8%) (Figures 2D−E and 3). The 2-hydroxy-3,3-dimethylbutan-2-yl group of buprenorphine engaged TM2 interactions, with A119$^{2.53}$, Q126$^{2.60}$, and Y130$^{2.64}$ for 22.3, 92.2, and 36.3% of the simulation time, respectively, whereas interactions with morphine for these residues were below 10% (Figure 3). This group, together with the 6-*O*-methyl ether, projected toward the extracellular loop 2 (ECL2), interacting with residues I146$^{3.29}$ and L221^{ECL2} for 39.3 and 20% of the time, respectively, whereas interactions with morphine were below 5% for both residues. N152$^{3.35}$ was the only residue showing a higher interaction frequency with morphine than buprenorphine, with 70.3 and 18.2% of the simulation time, respectively (Figures 2B,D and 3). Although interactions with some of these residues are lacking in the average structure depicted in Figure 2, MD simulations captured their involvement in stabilizing the ligands at the μOR orthosteric site.

We calculated hydrogen bonds and salt bridges to accurately differentiate the intermolecular interactions in the receptor/ligand complexes. Only a few residues formed hydrogen bonds with ligands, which include Y150$^{3.33}$ (1.88% for morphine and 2.68% for buprenorphine), K235$^{5.39}$ (16.22% for morphine and 0.32% for buprenorphine), and H299$^{6.51}$ (13.46% for morphine

https://doi.org/10.1021/acs.jcim.5c00078
J. Chem. Inf. Model. 2025, 65, 5071−5085

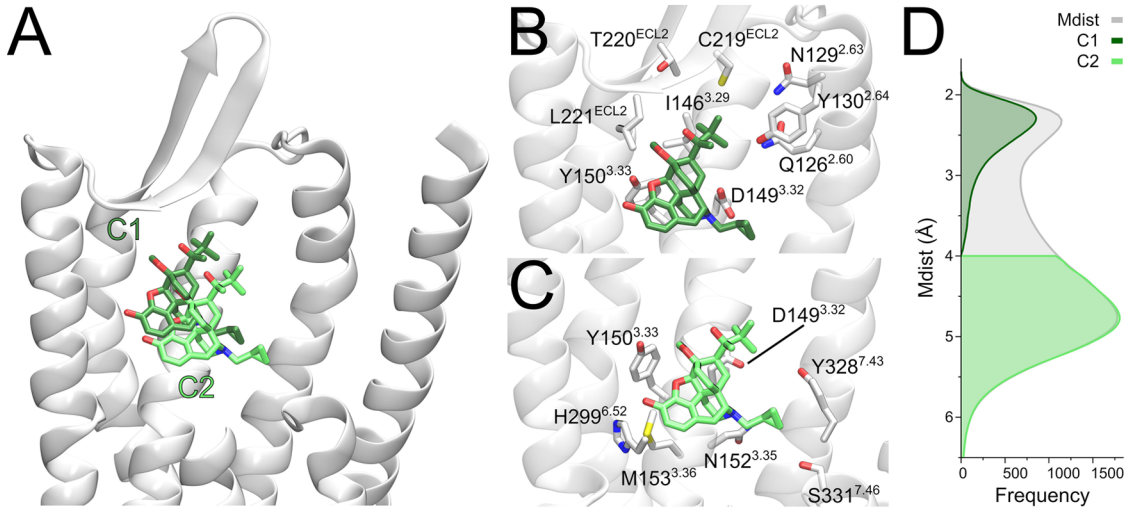

Figure 4. Distinct ligand−receptor interactions explored by buprenorphine during MD simulations. (A) Representative C1 and C2 interaction states of buprenorphine are depicted as dark and light green sticks, respectively, while the μOR is depicted as silver cartoons. μOR residues that stabilize (B) C1 and (C) C2 interaction states are illustrated as silver sticks. (D) The frequency of the minimum distance (Mdist, in gray) of buprenorphine to I146$^{3.29}$ or L221^{ECL2}, indicating C1 (dark green) and C2 (light green) interaction states. For a cleaner visualization, μOR residues from I300$^{6.53}$ to G327$^{7.42}$ were removed.

and 5.75% for buprenorphine). Although less frequent, these residues participated in water-mediated interactions for stabilizing both ligands (Figure S4A,B). Regarding the analysis of salt bridges with D149$^{3.32}$ of the receptor, we found that morphine had more frequent interactions, accounting for 97.28%, compared to only 29.58% for buprenorphine. The percentages of contacts, hydrogen bonds, and salt bridges of μOR residues with morphine or buprenorphine are shown in Table S2.

Buprenorphine Exhibits Broader Exploration at the μOR Orthosteric Site. We noticed that buprenorphine, unlike morphine, interacted with ECL2 residues, as mentioned above. This allowed us to discriminate between two sets of buprenorphine interactions, considering residues I146$^{3.29}$ and L221^{ECL2}, called C1 and C2. In C1, we considered interactions with both residues, whereas C2 was defined by the absence of interactions with these residues (Figure 4). C1 accounted for 16.5% of the simulation time, while C2 corresponded to 57.1%. The remaining 26.3% corresponded to contacts with I146$^{3.29}$ or L221^{ECL2}, considered an intermediate interaction state.

By examining the percentage of contacts for each ligand−receptor interaction state (Figure 4B−C), we observed that although near the D149$^{3.32}$ residue in both interaction states, buprenorphine's ammonium group forms remarkably more salt bridges in C1 (72.76%) compared to C2 (11.06%). Additionally, the interaction between Y150$^{3.33}$ and buprenorphine decreased in C2 (81.1%) compared to C1 (99.99%), also reducing hydrogen bonds from 8.83% to nearly zero (Table S2). Interestingly, although these interaction states maintain the same water-mediated interaction with Y150$^{3.33}$, K235$^{5.39}$, and H299$^{6.52}$, C2 presents a water molecule mediating interactions with D149$^{3.32}$, Y328$^{7.43}$, and buprenorphine's ammonium group (Figure S4C−D).

The C1 interaction state exhibited more frequent ECL2 interaction due to buprenorphine's 2-hydroxy-3,3-dimethylbutan-2-yl and 6-O-methyl ether groups, interacting with C219^{ECL2} and T220^{ECL2} for 30.3 and 26.6% of the simulation time, respectively, while such interactions were below 1% in C2 (Table S2). These residues, located above the μOR binding site, facilitated interactions with neighboring TM2 residues in C1, namely Q126$^{2.60}$, N129$^{2.63}$, and Y130$^{2.64}$, for 91.1, 16.6, and 61.9% of the time, respectively (Table S2). In contrast, C2 displayed buprenorphine more deeply in the orthosteric site, as evidenced by interactions with N152$^{3.35}$ (23.5%) and S331$^{7.46}$ (7.2%), whereas C1 displayed 11.7 and 0.4% interactions with the respective residues. It is noteworthy that interactions with TM2 (Q126$^{2.60}$), TM3 (M153$^{3.36}$), TM5 (K235$^{5.39}$ and V238$^{5.42}$), TM6 (I298$^{6.51}$, H299$^{6.52}$, and V302$^{6.55}$), and TM7 (T320$^{7.35}$, C323$^{7.38}$, I324$^{7.39}$, G327$^{7.42}$, and Y328$^{7.43}$) were consistent in both sets of buprenorphine interaction states. The percentages of contacts, hydrogen bonds, and salt bridges of buprenorphine in the C1 and C2 interaction states are shown in Table S2. The minimum distance between buprenorphine and residues I146$^{3.29}$ and L221^{ECL2} yielded two peaks, showing C1 as a subpopulation interacting with both residues and C2 exceeding the distance cutoff. Despite these structural differences observed in C1 and C2, we found in our MD simulations that both states oscillated rapidly between each other, being distinguished in only one of our replicas (Figure S5).

Metadynamics Suggests Distinct Ligand Binding Regions at the μOR Orthosteric Site. To further investigate the binding pose and intermediate interaction states of buprenorphine at the μOR orthosteric site, we selected a representative conformation from our MD simulations with the inactive conformation of the receptor for each complex. Then, we used the funnel-metadynamics technique to enhance ligand exploration, which has been successfully employed for reproducing experimental binding affinities and identifying intermediate binding sites in GPCRs.[62] Reported binding affinities for morphine range from −11.61 to −12.67 kcal/mol,[66,67] and for buprenorphine, from −12.52 to −13.71 kcal/mol.[66,68] Our predicted binding affinities converged to experiments after approximately 1 μs (Table S1), yielding average values of −11.63 kcal/mol (0.16 SD) for morphine and −12.68 kcal/mol (0.2 SD) for buprenorphine. The time-dependent free-energy values and profiles for both ligands,

https://doi.org/10.1021/acs.jcim.5c00078
J. Chem. Inf. Model. 2025, 65, 5071−5085

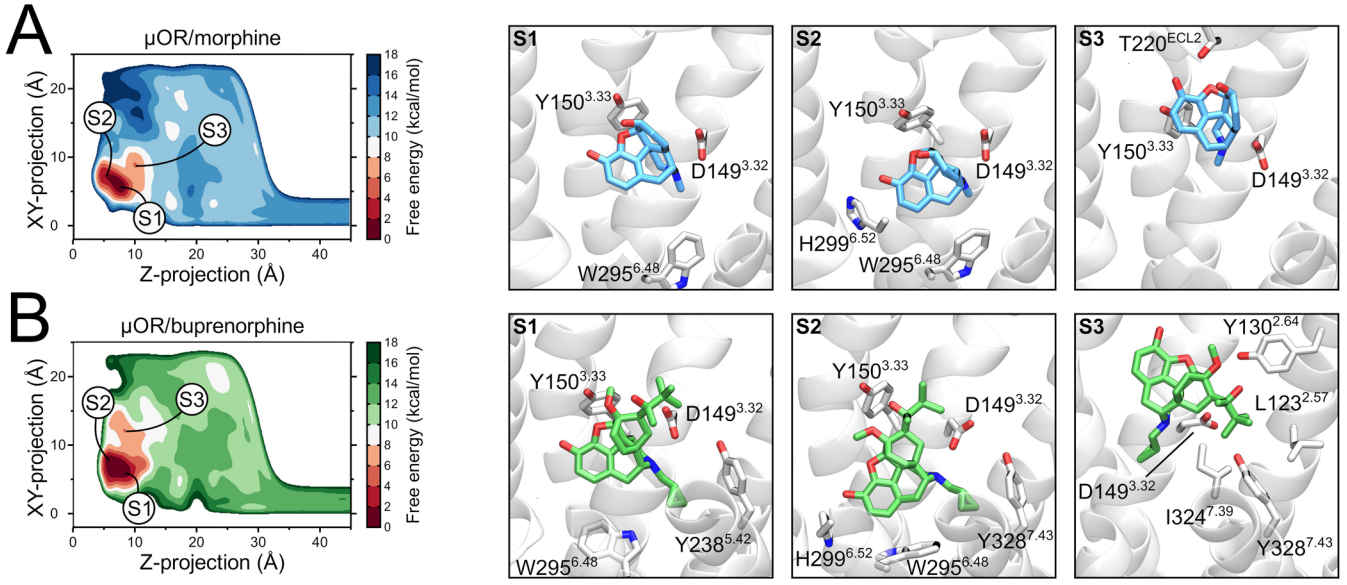

Figure 5. Determination of binding states for the μOR/morphine and μOR/buprenorphine complexes using funnel-metadynamics. The left panels display free energy surfaces for (A) morphine and (B) buprenorphine, highlighting S1, S2, and S3 substates for each complex. Contour lines are drawn every 2 kcal/mol. Representative ligand−receptor interactions for these substates are illustrated in the right panels, with μOR residues, morphine, and buprenorphine depicted as silver, cyan, and green sticks, respectively.

using the *Z*-projection, are shown in the Supporting Information (Figure S6).

The converged free-energy landscapes for morphine and buprenorphine highlight the minimum energy (S1 substate) at the same binding pose observed in classical MD simulations (Figure 2), validating the classical interactions for morphinan-scaffold ligands as previously discussed.[46] Both ligands explored a deeper region in the μOR orthosteric site (S2 substate) while preserving the salt bridge with D149$^{3.32}$. Interestingly, such an interaction was also observed in the C2 interaction state of buprenorphine from our classical MD simulation results. In contrast, each molecule exhibited a distinct exploration in the μOR orthosteric site. While morphine explored a restricted area directly above (*Z*-projection) the S1 substate, buprenorphine explored more extensively in both *XY*- and *Z*-projections (Figure 5, light red regions), leading to the identification of a third substate (S3 substate). In this substate, morphine maintained the salt bridge with D149$^{3.32}$ while visiting a vestibular secondary site above S1, stabilized by a hydrophobic region involving TM3 (I146$^{3.29}$) and TM6 (V302$^{6.55}$ and W320$^{7.35}$) residues (Figure S7). In contrast, the S3 substate of buprenorphine was localized to the side of S1, with its 2-hydroxy-3,3-dimethylbutan-2-yl group exploring a hydrophobic region formed by TM2 (L123$^{2.57}$ and Y130$^{2.64}$) and TM7 (I324$^{7.39}$ and Y328$^{7.43}$) residues (Figure S8).

Conformational Changes of the μOR Induced by Morphine and Buprenorphine. After a detailed description of the μOR interactions with morphine and buprenorphine, we were motivated to determine the local and global conformational changes induced by each ligand on the inactive conformation of the receptor. We compared the local changes with the experimental structures of the active (PDB code 6DDF)[69] and inactive (PDB code 7UL4)[65] conformations of the receptor from *Mus musculus*. In contrast, we assessed the global changes through MD simulations of the *apo*-μOR inactive conformation, performed under the same parameters as those including the ligands.

We identified two relevant local changes in the μOR induced by morphine or buprenorphine, particularly in the side chain dihedral angle orientations of residues Q126$^{2.60}$ and W295$^{6.48}$ during MD simulations (Figure 6). For Q126$^{2.60}$ (Figure 6A), the active and inactive experimental structures exhibit the side chain oriented toward the center of the orthosteric site despite presenting dihedral angles of 88.74 and 173.23°. Our MD simulations revealed that this residue adopts a distinct conformation in the presence of both ligands, with its side chain oriented toward the receptor's extracellular side, displaying dihedral angles concentrated around −60°. For W295$^{6.48}$ (Figure 6B), buprenorphine induced a broad distribution of dihedral angles, predominantly around −120°. This orientation, although negative compared to 106.51° in the experimental inactive conformation, can be related to the μOR's inactive conformation, where W295$^{6.48}$'s side chain projects toward the orthosteric site in the same direction, stabilizing interactions with the morphine-scaffold of buprenorphine. On the other hand, morphine induced W295$^{6.48}$ to explore dihedral angles around both the active and inactive experimental receptor conformations.

We next investigated μOR global conformational changes induced by morphine or buprenorphine, focusing on the distances between TM helices on both the extracellular and intracellular sides of the receptor (Figure 7), as these distances distinguish GPCR conformational states.[70] We found that both ligands stabilized the TM distances on the extracellular side of the receptor. The TM5-TM7 distance exhibited a single peak of around 25 Å for both ligands, compared to a diverse distribution (21−26 Å) with a high frequency of around 22 Å observed in the *apo*-μOR (Figure 7A). Similarly, the TM6-TM7 distance stabilized around 15.5 Å in the presence of both ligands, in contrast to a secondary peak of around 13 Å in the *apo*-μOR (Figure 7B). In contrast, the TM4-TM7 distance showed that morphine and the *apo*-μOR stabilized this distance around 29 Å, whereas buprenorphine induced an outward movement of TM7 on the extracellular side of the receptor, shifting this distance to a value of approximately 31 Å

https://doi.org/10.1021/acs.jcim.5c00078
J. Chem. Inf. Model. 2025, 65, 5071−5085

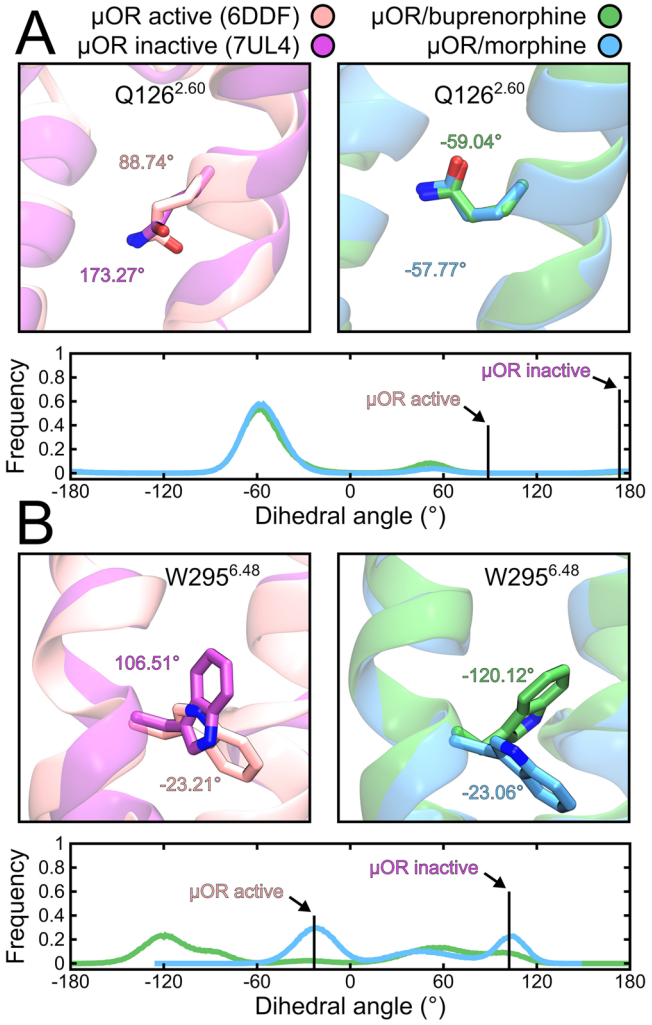

Figure 6. Dihedral angle distribution of μOR residues Q126$^{2.60}$ and W295$^{6.48}$ during MD simulations. Experimental and representative conformations obtained from MD simulations for (A) Q126$^{2.60}$ and (B) W295$^{6.48}$ side chain orientations are displayed in the upper panels, while frequency distributions are depicted in the lower panels. The angle distribution for morphine and buprenorphine are colored in cyan and green, respectively. Experimental μOR active and inactive conformations are colored in salmon and purple, respectively, with experimental values indicated by vertical bars. μOR TM helices and residues are represented as cartoons and sticks, respectively.

(Figure 7C). Looking at the intracellular side of the receptor, we observed that TM2-TM5 and TM3-TM7 distances exhibited a similar distribution in both the *apo*-μOR and the buprenorphine-bound receptor, with frequencies stabilized around 26 and 24 Å, respectively. On the other hand, morphine led to a decrease in both distances, with peaks around 24 Å and 21.5 Å for TM2-TM5 and TM3-TM7 distances, respectively, indicating an inward movement of TM5 and TM7.

The distinct TM arrangements on the extracellular side of the μOR suggest that morphine and buprenorphine contribute to stabilizing the shape of the μOR orthosteric site. To validate this hypothesis, we measured the volume of the μOR orthosteric site using the Epock software[71] of all frames collected from MD simulations (Figure 8). As expected, the *apo*-μOR exhibited high volume fluctuations of its orthosteric site, with a median volume of 33.4 × 100 Å^3 and an interquartile range (IQR) of 10.07 × 100 Å^3. In contrast, buprenorphine led to a median volume of 40.19 × 100 Å^3 and IQR of 5.80 × 100 Å^3 values, while morphine-associated volumes were 35.59 × 100 Å^3 for the median and 6.25 × 100 Å^3 for the IQR. Furthermore, the analysis of buprenorphine interaction states revealed that C1 displayed values similar to those morphine-induced, with a median of 36.60 × 100 Å^3 and IQR of 5.79 × 100 Å^3. In contrast, C2 showed slightly higher median values of 41.63 × 100 Å^3, and IQR of 5.13 × 100 Å^3.

DISCUSSION

The potential use of opioid drugs to manage chronic pain has opened a new avenue for the development of safer and more effective opioid medications that exhibit biased[15] or partial[27] agonism at the μOR. In this scenario, the identification of structural determinants related to these functional effects is crucial for developing opioid drugs with reduced unwanted side effects.[44,46] A recent model for explaining biased agonism at the μOR toward G protein pathways suggests that strong D149$^{3.32}$ and Y328$^{7.43}$ interactions lead to arrestin recruitment. In contrast, weak D149$^{3.32}$ and strong Y150$^{3.33}$ interactions are associated with reduced β-arrestin recruitment.[51] This proposal was further supported by evidence indicating that weak TM6 and TM7 interactions contribute to biased agonism at the μOR.[46] However, Wang and collaborators[20] argued that this model fails to explain the biased agonism effect of PZM21, which exhibits a strong Y328$^{7.43}$ interaction. Making the debate even more controversial, the experimental structure of the antagonist alvimopan bound to the μOR revealed that its phenyl group extended into a hydrophobic subpocket formed by TM2 and TM3, similar to full agonists such as fentanyl or DAMGO, but with weak TM6 and TM7 interactions.[65] In the present work, we observed that buprenorphine exhibits a slightly weaker interaction with Y150$^{3.33}$ compared to morphine while engaging strong D149$^{3.32}$, TM6, and TM7 interactions. Ribeiro and collaborators[61] reported similar findings using infrequent metadynamics to determine buprenorphine's dissociation from the μOR. Considering recent findings that classify buprenorphine as a partial and G protein-biased agonist at the μOR,[31,42,43] the determination of structural aspects related to its functional effects remains necessary. Furthermore, a recent study showed that buprenorphine induces conformational changes of the μOR similar to those of other G protein-biased agonists such as TRV130, PZM21, and MP.[72] Chemical structures of relevant partial or biased agonists are shown in Figure S9, facilitating the comparison with morphine and buprenorphine. We delved deeper into the dynamic behavior of buprenorphine using classical MD simulations and metadynamics, aiming to uncover relevant structural aspects that shed light on the current knowledge of partial and biased agonism in the μOR.

A recent study elucidated the experimental structure of morphine bound to the μOR by cryo-EM, highlighting a salt-bridge formation with D149$^{3.32}$ and a hydrogen bond with the Y150$^{3.33}$ residue of the receptor.[46] Such interactions are found in several experimental structures of morphinan-scaffold ligands bound not only to the μOR,[44,45,47,48] but also to δOR[73,74] and κOR.[44,75] Computational studies have identified similar molecular interactions for other opioid ligands, including buprenorphine.[43,50,61] These interactions were covered in our MD simulations (Figure 2) and metadynamics (Figure 5) results. We also found water-mediated interactions stabilizing the complexes (Figure S4), as reported by previous

https://doi.org/10.1021/acs.jcim.5c00078
J. Chem. Inf. Model. 2025, 65, 5071−5085

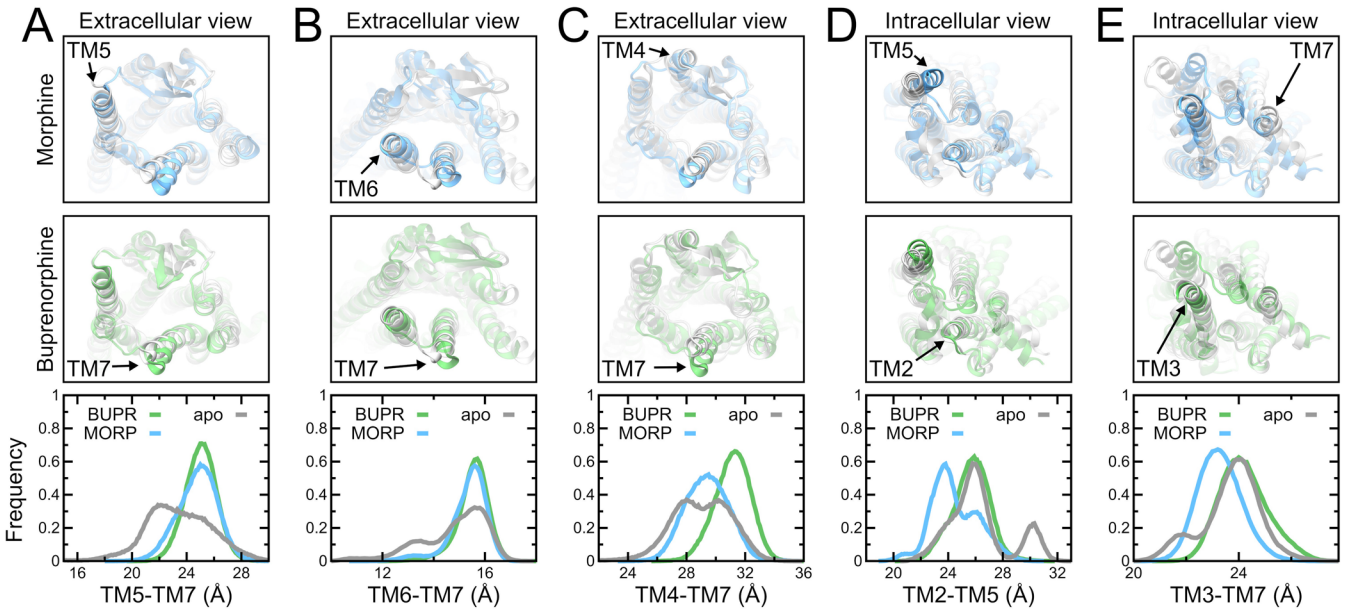

Figure 7. Global conformational changes in the μOR during MD simulations. Relevant (A−C) extracellular and (D, E) intracellular TM distances of the μOR in the *apo*-form (APO), morphine-bound (MORP), and buprenorphine-bound (BUPR) are depicted in silver, cyan, and green, respectively. μOR conformations are illustrated as cartoons and have been superposed onto the *apo*-μOR (silver) to show structural alterations induced by (top panel) morphine (cyan) and (middle panel) buprenorphine (green). The frequency distributions of TM distances are shown in the lower panels, following the same color pattern.

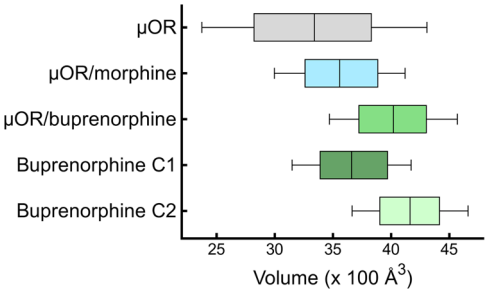

Figure 8. Volume of the μOR orthosteric site during MD simulations. Boxplots represent the volume of the μOR unbound (silver) and bound to morphine (cyan) or buprenorphine (green), including buprenorphine interaction states C1 (dark green) and C2 (light green). For the sake of visual simplicity, the 80% of the data closest to the median were considered for plotting.

research.[20,45,47,51,53,69] Interestingly, experimental data suggest that buprenorphine exhibits a stronger binding affinity compared to morphine.[66,76,77] Our binding affinity calculations are in line with the experimental binding energy range for both ligands, indicating that buprenorphine has a stronger binding energy of approximately 1 kcal/mol. This aspect may reflect the presence of buprenorphine's additional chemical groups, such as the *N*-methylcyclopropyl and 2-hydroxy-3,3-dimethyl-butan-2-yl, resulting in stronger interactions with TM2, TM3, TM7, and ECL2 compared to morphine. Additionally, the solvated and unrestrained conditions of our funnel-metadynamics results account for the known interplay between conformational entropy and solvation entropy in ligand binding.[78] In this context, the desolvation of these predominantly hydrophobic groups upon receptor binding may also contribute to buprenorphine's stronger binding affinity compared to morphine.

The identification of distinct binding regions in GPCRs has been essential in identifying several GPCR pharmacophores, linking specific regions to efficacy ("message") and selectivity ("address").[79] Subsequent work has shown that chemical modifications can convert agonists into antagonists,[80] providing insights into the rational selectivity and functional modulation of opioid receptors.[45,47,73] Thus, the chemical substitutions present in buprenorphine certainly play a role in elucidating its functional effect on the μOR. Understanding these structure−function aspects is essential to better describe the mechanisms underlying opioid receptor modulation.[81]

Another remarkable pharmacological property of buprenorphine is its longer residence time compared to other μOR agonists such as DAMGO, morphine, loperamide, and the TRV130 enantiomers. This binding kinetics profile, which may explain the long-lasting analgesia of buprenorphine, is not related to biased agonism, since the two strongly G protein-biased μOR agonists buprenorphine and TRV130 possess very different residence times, with that of buprenorphine being 18-fold longer than that of TRV130.[42] Previous research using infrequent metadynamics successfully reproduced experimental dissociation rates for morphine and buprenorphine and identified distinct transitional states for these ligands.[61] In our study, the application of funnel-metadynamics enhanced the ligand conformational exploration into the μOR orthosteric site, allowing the identification of intermediate binding states for these ligands. We found that the S3 substate for morphine identified in our work is similar to the "vestibular region state" described by Ribeiro and collaborators,[61] where the ligand stabilized above the region corresponding to the S1 substate through the classical salt bridge with D149$^{3.32}$ and hydrophobic interactions (Figures 5 and S7). In contrast, our findings for buprenorphine revealed unique intermediate binding states. First, we did not observe a conformation describing buprenorphine's upside-down orientation into the μOR orthosteric site reported by Ribeiro and collaborators,[61] identified as an "alternative bound state". Second, the "vestibular region state" identified by Ribeiro and collabo-

https://doi.org/10.1021/acs.jcim.5c00078
J. Chem. Inf. Model. 2025, 65, 5071−5085

rators[61] shows buprenorphine's cyclopropyl group accessing a hydrophobic region between TM2 and TM7, while our corresponding state (S3 substate) shows the 2-hydroxy-3,3-dimethylbutan-2-yl group occupying this area. This region also accommodates the indole ring of the partial and biased agonist MP[21] (Figure S8) and was recently identified as part of an allosteric site for the μOR negative allosteric modulator 368.[48] Furthermore, our analysis of the free-energy landscape for both ligands demonstrates that buprenorphine exhibits a broader exploration into the μOR binding site (Figure 5, dark red regions), attributed to the enrichment of lower values onto the *Z*-projection (around 60 Å) of the S2 substate compared to morphine (Figure S6). Buprenorphine also explored a broader area onto both collective variables (CVs) (Figure 5, light red and white regions), likely linked to its prolonged residence time. Although our study did not directly measure dissociation rate constants, our results present insights into the mechanism underlying buprenorphine's longer residence time and identify intermediate states that may be related to other ligands with similar pharmacological profiles, illuminating the complex pharmacology of buprenorphine at the μOR.

Classical MD simulations are widely used to explore the structural aspects of ligand-GPCR complexes by capturing local motions of side chain arrangements, thereby providing functional insights into these receptors. For instance, a stable $Q126^{2.60}$–$Y328^{7.43}$ interaction is associated with balanced and full agonist efficacy, whereas biased and partial agonists, such as MP, fail to stabilize such an interaction.[21] $Q126^{2.60}$ has been identified as critical for biasing signaling at μOR, with a $Q126^{2.60}$A mutant diminishing arrestin recruitment.[21] The orientation of the $Q126^{2.60}$ side chain, either toward the μOR orthosteric site to enable $Y328^{7.43}$ interaction or toward the receptor's extracellular side,[56] can be influenced by ligands that target a hydrophobic subpocket called sp1 formed by TM2, TM3, and ECL1 located above $Q126^{2.60}$ thereby stabilizing the $Q126^{2.60}$–$Y328^{7.43}$ interaction.[21] In our study, buprenorphine exhibited a strong interaction with $Q126^{2.60}$, which was not observed for morphine (Figure 3). These results contrast with a previous study that reported a weaker $Q126^{2.60}$ interaction with buprenorphine and no interaction with morphine, even when using a higher cutoff to determine atomic contacts.[61] These differences could arise from the utilization of enhanced-sampling techniques, forcing the system to a broader exploration than classical MD simulations in the present work. We attribute buprenorphine's interaction with $Q126^{2.60}$ to its 2-hydroxy-3,3-dimethylbutan-2-yl chemical group (Figure 2).[21] Despite this, our MD simulations indicate that neither buprenorphine nor morphine prevented the rotation of the $Q126^{2.60}$ side chain, even when MD simulations started from the receptor's active conformation (Figure S10), similarly to that observed by Ricarte and collaborators.[56] Additionally, our classical MD simulations indicated that although buprenorphine interacts with $Q126^{2.60}$, it does not occupy the sp1 subpocket identified by Qu and collaborators,[21] as evidenced by the absence of interactions with residues deeper in the pocket, such as $W135^{ECL1}$ (Table S2). Although previous studies suggest that small molecules interacting within the sp1 pocket are linked to enhanced opioid potency, as observed with DAMGO, BU72, and fentanyl,[46,47,69] partial agonists such as TRV130, PZM21, or FH210,[20,46] and even the antagonist BU74,[47] have accessed this region. Interestingly, experimental structures of the μOR bound to the agonist morphine[46] or the irreversible antagonist β-funaltrexamine (β-FNA)[45] also revealed the $Q126^{2.60}$–$Y328^{7.43}$ interaction, even if these ligands do not access the sp1 subpocket. Therefore, relating the side chain orientation of $Q126^{2.60}$ and μOR conformational states may be puzzling, requiring further studies to clarify its precise role in μOR activation.

Despite the debate on the participation of $W295^{6.48}$ in forming a toggle switch that distinguishes GPCR conformational states,[82,83] we observed that both morphine and buprenorphine highly influenced the side chain rotameric distribution of $W295^{6.48}$. Morphine induced a constrained distribution of $W295^{6.48}$ dihedral angles with two distinct peaks, whereas buprenorphine led to a broader dihedral angle distribution (Figure 6), also observed when simulations started from the μOR's active conformation (Figure S10). Previous work suggested that buprenorphine fails to stabilize $W295^{6.48}$ in a unique orientation compared to other agonists,[43] agreeing with our work. The diminished $Y150^{3.33}$ interactions and salt bridges with $D149^{3.32}$ may allow buprenorphine to visit regions deeper into the orthosteric pocket of the receptor, as shown by the percentage of contacts (Figure 3 and Table S2). In addition, our metadynamics results suggest that the exchange from buprenorphine's furan-ring oxygen to its 6-*O*-methyl ether when interacting with $Y150^{3.33}$ could stabilize these deeper conformations (Figure 5). This interaction may enhance the contact between buprenorphine and $W295^{6.48}$, inducing diverse residue side chain orientations. Reinforcing our results, the observed weaker $Y150^{3.33}$ interaction with buprenorphine could explain why site-directed mutagenesis of this residue has a slight reduction in buprenorphine's binding affinity at the μOR while considerably affecting morphine.[84] Moreover, the cleavage of the cyclopropyl group converts buprenorphine into the agonist norbuprenorphine[85] and the antagonist BU74 into the agonist BU72,[47] which may also explain the antagonist effect of naltrexone at the μOR along with other low-efficacy ligands.[86] Therefore, it is reasonable to infer that these structural aspects of buprenorphine contribute to its low efficacy at the μOR.

Recent computational studies have suggested that ligands may drive the μOR active conformation toward distinct intermediate states, with biased agonists maintaining TM orientations similarly to those in the active (G protein-bound) conformation, leading to preferential activation of G protein pathways, while balanced full agonists might reduce some TM distances to enhance interaction with β-arrestins.[21,46] Changes in $L112^{2.46}$–$P335^{7.50}$[21] and $I280^{6.33}$–$E343^{8.48}$[46] distances are referred to as essential for discriminating between balanced full and biased partial agonists at the μOR. To assess buprenorphine's impact on these distances, we analyzed the structural effects of morphine and buprenorphine starting from the μOR active conformation (Figure S11). Our findings indicate that morphine reduces the $L112^{2.46}$–$P335^{7.50}$ distance to a primary peak at 8.5 and a secondary small peak at 6 Å, while buprenorphine maintains this distance around the active conformation at 8.5 Å (Figure S11), agreeing with observations by Qu and collaborators.[21] Conversely, while morphine stabilized the $I280^{6.33}$–$E343^{8.48}$ distance around the active conformation, buprenorphine exhibited a primary peak at this active conformation and a secondary peak at a shorter distance (Figure S11). This observation diverges from results reported by Zhuang and collaborators,[46] likely due to their shorter (1.5 μs in total) MD simulations compared to our more extensive 5-fold data, which allowed for an extended conformational sampling. Taken together, our structural analyses suggest that

https://doi.org/10.1021/acs.jcim.5c00078
J. Chem. Inf. Model. 2025, 65, 5071−5085

morphine induces the μOR into an alternative conformation similar to those obtained by full and balanced agonists, such as fentanyl and DAMGO. In contrast, buprenorphine appears to maintain the receptor's canonical active conformation, behaving similarly to the partial and biased agonist MP.

Ligand-induced shifts in GPCR conformational states can restrict GPCR conformational sampling toward intermediate conformations, likely favoring receptor activation or inactivation.[12,70] In addition, spectroscopy studies have demonstrated that ligands with distinct functional effects induce unique GPCR conformational changes.[43,72,87] In the present work, we observed that morphine and buprenorphine stabilize extracellular TM distances relative to the unbound receptor (Figure 7). Moreover, our results indicate that morphine induces an inward movement of TM5 and TM7 in the receptor's intracellular side (Figure 7). Although previous studies reported similar results for intracellular TM5 rearrangements induced by morphine,[52,56] its relationship with the dihedral rotation of W295$^{6.48}$ seems most likely due to residue stabilization (Figure 6), limiting the μOR conformational sampling, as the unbound receptor explores a broad range of TM2-TM5 distance (Figure 7). Buprenorphine induced a TM7 outward movement in the receptor's extracellular side (Figure 7), which was also found by Bartuzi and collaborators.[54] We attribute this conformational shift to an increased volume of the orthosteric site compared to morphine (Figure 8). Detailed analysis revealed that this outward movement was more pronounced when buprenorphine formed weak salt bridges with D149$^{3.32}$ and hydrogen bonds with Y150$^{3.33}$ (C2 interaction state), broadly exploring the receptor's orthosteric site (S2 substate). This suggests a unique buprenorphine structural effect that can be related to partial agonism at the μOR. Additionally, our classical MD and metadynamics simulations highlighted buprenorphine's interaction with ECL2 residues, which is associated with strong salt bridges with D149$^{3.32}$, as identified in the C1 interaction state (Table S2). Such ECL2 interactions were identified as essential for biasing μOR signaling, as observed with several morphinan-scaffold ligands.[44] Consistent with this, biased agonists such as PZM21 and FH210 show interactions with ECL1 and ECL2.[20] NMR experiments also revealed that buprenorphine induces a slightly more pronounced ECL2 conformational change compared to other partial biased agonists (TRV130 and PZM21) or full balanced agonists (DAMGO and BU72),[43] which could be related to the residue interaction and conformational changes induced by buprenorphine observed in our work. Thus, sustained by previous works, our results indicate that 2-hydroxy-3,3-dimethylbutan-2-yl and 6-*O*-methyl ether groups of buprenorphine are responsible for a stronger ECL2 interaction, likely related to its biased agonism toward G protein signaling pathways.

In this study, we employed computational methods to elucidate relevant structural aspects of buprenorphine that explain its unique pharmacological effect on the μOR. Our approach aligns with recent findings, analyzing the critical role of the interaction between GPCR residues and ligands in the induction of specific pharmacological effects.[88] Such interactions induce specific receptor conformational changes,[72] activating a specific intracellular network of proteins and further distinct cellular responses.[89] The identification of key residues is essential for advancing our understanding of GPCR pharmacology. When compared to morphine, we found that the additional chemical groups in buprenorphine interact with distinct μOR regions to provide partial and biased agonist effects. In fact, partial and biased agonism are related properties in the sense that the inclusion of an additional signaling pathway implies a reduction in efficacy in the reference pathway, which then leads to partial agonism. This pharmacological behavior can be quantitatively simulated by using the three-state model of agonist action, in which two active receptor states (R* and R**) linked to two signaling pathways are included.[90] Partial agonism may also arise from a structural deficiency of the ligand-bound receptor active conformation in binding and activating the transducer protein or, if we consider time, a shorter or longer residence time of the ligand in the active or inactive receptor conformation, respectively. To conclude, this work presents a computational analysis for understanding the structural basis of buprenorphine's pharmacological effects at the μOR, which can contribute to the advancement of research in opioid drug design.

METHODS

Molecule Preparation. The human μOR (UniProt code P35372) (https://www.uniprot.org/) in its inactive conformation was built by homology modeling using the SWISS-MODEL web server.[91] The mouse μOR was used as a template (PDB code 7UL4),[65] which exhibits 98% sequence coverage and 93.9% sequence identity. The human μOR active conformation was retrieved from the cryo-EM structure (PDB code 8EF6),[46] preserving only receptor and morphine atoms. The protonation state of the μOR structures was calculated at a physiological pH of 7.4 using the PROPKA3 web server.[92] Morphine and buprenorphine structures were built using the Ligand Reader tool available on the CHARMM-GUI web server,[93] maintaining their amino group protonated to reproduce physiological pH conditions.

Molecular Docking. Molecular docking was performed by covering the μOR orthosteric site with a box of 80 × 80 × 80 *XYZ* grid points with a spacing of 0.375 Å using the AutoDockTools v.1.5.6 workspace.[94] Buprenorphine was docked to the μOR active and inactive conformations, while morphine was docked only to the receptor inactive conformation since the active conformation bound to morphine is experimentally known (PDB code 8EF6).[46] The receptor and ligands were converted to PDBQT format, preserving their protonation states. Subsequently, morphine and buprenorphine were docked into the μOR orthosteric site using AutoDock-GPU,[64] with the parameters for population size, number of runs, and number of evaluations set to 1000, 1000, and 30,000,000.

MD Simulations. We used the CHARMM-GUI web server[95] to prepare systems for every complex, including the *apo*-μOR in active and inactive conformations. A disulfide bond was patched to cysteines C142$^{3.25}$ and C219^{ECL2} to the receptor's active and inactive conformations, and an *S*-palmitoyl lipidation was included in C353$^{8.58}$ to the inactive conformation. Ligand force field parameters were obtained from the CHARMM General Force Field (CGenFF) program.[96] Each complex was placed in a hexagonal box and embedded in a POPC bilayer to obtain an initial system size of approximately 82 × 82 × 119 Å^3 in *XYZ* dimensions. Subsequently, each system was solvated with TIP3P water models and neutralized with potassium and chloride ions to reach a 0.15 M concentration. Initial input parameters for MD simulations were prepared to match with GROMACS

https://doi.org/10.1021/acs.jcim.5c00078
J. Chem. Inf. Model. 2025, 65, 5071−5085

v.2022.2[97] under the Charmm36m force field.[98] First, a minimization step was performed using the Steepest Descent algorithm until reaching an energy below 1000 kJ/mol/nm. Further, successive equilibration steps were performed according to the parameters specified in the Supporting Information (Table S3). Briefly, velocities were randomly generated according to a Maxwell−Boltzmann distribution at 310 K using the V-Rescale thermostat.[99] The Parrinello−Rahman barostat monitored the system pressure at 1 bar.[100] Position restraint forces applied on receptor backbone, side chain, ligand non-hydrogen, and lipid head atoms were progressively reduced to zero. Production was performed in four independent replicas lasting 2 μs for each system, collecting frames every 20 ps, for an amount of 48 μs (Table S1). Nonbonded interactions were calculated up to a distance of 10 Å, with a switching-force function between 10 and 12 Å. Long-range electrostatic interactions were calculated within a 12 Å cutoff using the particle-mesh Ewald (PME) method.[101]

Funnel-Metadynamics. Metadynamics simulations were conducted to estimate ligand binding affinity and identify intermediate states in the μOR's inactive conformation using GROMACS v2019.6[97] patched with PLUMED v2.8.1.[102] MD parameters were set as for classical MD simulations, described above. We employed well-tempered (WT) metadynamics[103,104] in combination with funnel-shaped constraints to limit ligand exploration in the solute for enhanced convergence. The frame with the lowest RMSD relative to the average structure of the μOR/morphine and μOR/buprenorphine complexes obtained from MD simulations was resubmitted to CHARMM-GUI to increase the system's Z-axis and allow ligand exploration in the unbound state; subsequently, the equilibration process was followed as previously described (Table S3). For each complex, the equilibrated system was used as the starting point for funnel-metadynamics simulations. Following a previous protocol,[62,105] we defined a distance between the Cα carbon of W295$^{6.48}$ and the nearest atoms of the ligand's center of mass to determine two CVs for metadynamics: one aligned onto the Z-axis (Z-projection) and the second onto the XY-plane (XY-projection), parallel to the membrane. The funnel-like restraint[62,106] was applied according to the following equation

$$r = h \cdot \frac{1}{1 + e^{s(z - z_0)}} + b$$

where r denotes the XY-projection, h = 22 Å the funnel width, s = 80 Å^{-1} the funnel steepness, z is the Z-projection, z_0 = 30 Å the inflection point of the funnel, and b = 2.5 Å the minimum funnel width. A quadratic repulsive potential force of 1000 kJ/mol and upper and lower walls set at 50 and 4 Å in the Z-projection, respectively, prevented the ligand from crossing the funnel boundaries.

We performed an initial metadynamics simulation to extract 24 representative structures for each 2 Å window along the Z-projection to use as starting points for multiple walkers (Raiteri et al.).[107] Gaussian hills parameters height and width were set to 2 kJ/mol and 1 Å, respectively, with a bias factor of 20 applied at every 1000 steps. Subsequently, a metadynamics history-dependent bias was applied, rescaling Gaussian hills height and bias factor to 1 kJ/mol and 10, respectively, until reaching WT metadynamics convergence. Free energies were calculated by summing the Gaussians using the sum_hills function from the PLUMED plugin,[102] correcting the loss of translational and rotational freedom of the ligand in the unbound state imposed by funnel boundaries, according to the protein−ligand binding free energy equation

$$\Delta G = -\kappa_B T \ln(K_b C^0)$$

where κ_B is the Boltzmann constant, T is the temperature of the system, and C^0 = 1/1660 Å^{-3} is the standard concentration. The binding constant K_b is defined as

$$K_b = \int_{\text{bound}} dz\, e^{[-((W_{(z)} - W_{\text{ref}})/\kappa_B T)]} \pi R_{\text{cyl}}^2$$

where z is the coordinate along Z-projection, while $W(z)$ and W_{ref} correspond to the free energy in the bound and unbound states, respectively. We used the integral and average of free energy values over the bound and unbound states, respectively. πR_{cyl}^2 is the surface of the cylinder determined by its radius (R), accounting for the volume correction for the funnel restraint potentials described by Limongelli and collaborators.[108] The funnel shape determined in our work led to a cylinder with a radius of 2.5 Å in the unbound region, defined from 45 to 48 Å along the Z-projection, resulting in a correction value of 1.32 kcal/mol. Metadynamics simulations were performed until the free energy landscapes converged, which occurred after 0.9 and 1.3 μs for morphine and buprenorphine, respectively. Average and standard deviation of binding affinities for morphine and buprenorphine were calculated using the last 300 ns of metadynamics simulation, sampled every 1 ns.

Structural Analysis. RMSD calculations were carried out using GROMACS built-in functions. The average structure of each replica was obtained using the GROMACS plugin *gmx cluster*, considering all protein/ligand atoms. TM distances were determined by calculating the center of mass of the four Cα atoms of each extracellular and intracellular extremities of the receptor. Dihedral angle calculations for Q126$^{2.60}$ and W295$^{6.48}$ were conducted using the atomic sequences CA-CB-CG-CD and CA-CB-CG-CD1, respectively. The percentage of contacts was calculated considering atomic distances within a 4 Å cutoff, and salt bridges were calculated considering the minimum distance between the nitrogen atom of ligand amino groups and the side chain oxygens of D149$^{3.32}$ less than 4 Å. These calculations were performed using VMD built-in functions or scripting.[109] Hydrogen bonds were calculated using the VMD plugin *hbonds*, defining only polar atoms (N, O, and S) as donors (D) or acceptors (A), with the D−A distance less than 3.2 Å and the D-H-A angle less than 50° to capture strong and moderate hydrogen bonds.[110] Water-mediated interactions were identified by calculating the occupancy of water molecules after aligning receptor backbone atoms, using the VMD plugin *volmap* with a map resolution of 0.5 Å. Volume calculations were performed using Epock,[71] covering the μOR orthosteric site with a sphere radius and grid spacing of 15 and 0.5 Å, respectively. All structural illustrations were generated with VMD,[109] and all graphs were built using gnuplot v.5.2 (http://www.gnuplot.info).

■ ASSOCIATED CONTENT

Data Availability Statement

All input files necessary to reproduce our classical MD and funnel-metadynamics simulations, including treated trajectories and metadynamics outputs (HILLS and COLVAR files), are freely available at 10.5281/zenodo.14676141.

https://doi.org/10.1021/acs.jcim.5c00078
J. Chem. Inf. Model. 2025, 65, 5071−5085

Supporting Information

The Supporting Information is available free of charge at https://pubs.acs.org/doi/10.1021/acs.jcim.5c00078.

Best pose for the μOR/buprenorphine obtained from molecular docking (Figure S1); RMSD calculations for non-hydrogen atoms of morphine and buprenorphine (Figure S2); average conformations for μOR/morphine and μOR/buprenorphine complexes (Figure S3); water-mediated interactions (Figure S4); buprenorphine interaction states (Figure S5); binding free energy computed by funnel-metadynamics (Figure S6); S3 substate for the μOR/morphine complex obtained from funnel-metadynamics simulations (Figure S7); S3 substate for the μOR/buprenorphine complex obtained from funnel-metadynamics simulations (Figure S8); chemical structures of biased and partial agonists at the μOR (Figure S9); dihedral angle distribution of $Q126^{2.60}$ and $W295^{6.48}$ residues in the active μOR conformation (Figure S10); intracellular distances of the μOR in the active conformation (Figure S11); overview of the simulations performed (Table S1), percentage of contacts in μOR/ligands complexes (Table S2), and the equilibration protocol (Table S3) (PDF)

AUTHOR INFORMATION

Corresponding Author

Jesús Giraldo − *Laboratory of Molecular Neuropharmacology and Bioinformatics, Unitat de Bioestadística and Institut de Neurociències, Universitat Autònoma de Barcelona, 08193 Bellaterra, Spain; Unitat de Neurociència Traslacional, Parc Taulí Hospital Universitari, Institut d'Investigació i Innovació Parc Taulí (I3PT), Institut de Neurociències, Universitat Autònoma de Barcelona, 08193 Bellaterra, Spain; Instituto de Salud Carlos III, Centro de Investigación Biomédica en Red de Salud Mental, CIBERSAM, 28029 Madrid, Spain;* orcid.org/0000-0001-7082-4695; Email: Jesus.Giraldo@uab.cat

Author

Antoniel A. S. Gomes − *Laboratory of Molecular Neuropharmacology and Bioinformatics, Unitat de Bioestadística and Institut de Neurociències, Universitat Autònoma de Barcelona, 08193 Bellaterra, Spain; Unitat de Neurociència Traslacional, Parc Taulí Hospital Universitari, Institut d'Investigació i Innovació Parc Taulí (I3PT), Institut de Neurociències, Universitat Autònoma de Barcelona, 08193 Bellaterra, Spain; Instituto de Salud Carlos III, Centro de Investigación Biomédica en Red de Salud Mental, CIBERSAM, 28029 Madrid, Spain;* orcid.org/0000-0002-1278-7838

Complete contact information is available at: https://pubs.acs.org/10.1021/acs.jcim.5c00078

Author Contributions

A.A.S.G. conceived, designed, performed the research, analyzed data, and wrote the manuscript; J.G. conceived and designed the research and reviewed the manuscript. Both authors have given approval to the final version of the manuscript.

Funding

This project has received funding from Ministerio de Ciencia, Innovación y Universidades, Spain (MCIN/AEI/10.13039/501100011033) under grant number PID2020−119136RB-I00.

Notes

The authors declare no competing financial interest.

ACKNOWLEDGMENTS

This work was partially supported by the grant PID2020-119136RB-I00 funded by MCIN/AEI/10.13039/501100011033. The authors thankfully acknowledge RES resources provided by BSC in CTE-AMD to BCV-2023-2-0009.

REFERENCES

(1) Cohen, S. P.; Vase, L.; Hooten, W. M. Chronic Pain: An Update on Burden, Best Practices, and New Advances. *Lancet* **2021**, *397* (10289), 2082−2097.

(2) van Hecke, O.; Torrance, N.; Smith, B. H. Chronic Pain Epidemiology and Its Clinical Relevance. *Br. J. Anaesth.* **2013**, *111* (1), 13−18.

(3) Stein, C. Opioid Receptors. *Annu. Rev. Med.* **2016**, *67* (1), 433−451.

(4) Mattson, C. L.; Tanz, L. J.; Quinn, K.; Kariisa, M.; Patel, P.; Davis, N. L. Trends and Geographic Patterns in Drug and Synthetic Opioid Overdose Deaths—United States, 2013−2019. *MMWR. Morb. Mortal. Wkly. Rep.* **2021**, *70* (6), 202−207.

(5) NIDA. Drug Overdose Deaths: Facts and Figures, 2024. https://nida.nih.gov/research-topics/trends-statistics/overdose-death-rates. (accessed November 02, 2024).

(6) Manchikanti, L.; Singh, V. M.; Staats, P. S.; Trescot, A. M.; Prunskis, J.; Knezevic, N. N.; Soin, A.; Kaye, A. D.; Atluri, S.; Boswell, M. V.; Abd-Elsayed, A.; Hirsch, J. A. Fourth Wave of Opioid (Illicit Drug) Overdose Deaths and Diminishing Access to Prescription Opioids and Interventional Techniques: Cause and Effect. *Pain Physician* **2022**, *25* (2), 97−124.

(7) Gilron, I.; Jensen, T. S.; Dickenson, A. H. Combination Pharmacotherapy for Management of Chronic Pain: From Bench to Bedside. *Lancet Neurol.* **2013**, *12* (11), 1084−1095.

(8) Martin, W. R.; Eades, C. G.; Thompson, J. A.; Huppler, R. E.; Gilbert, P. E. The Effects of Morphine- and Nalorphine- like Drugs in the Nondependent and Morphine-Dependent Chronic Spinal Dog. *J. Pharmacol. Exp. Ther.* **1976**, *197* (3), 517−532.

(9) Spain, J.; Roth, B.; Coscia, C. Differential Ontogeny of Multiple Opioid Receptors (Mu, Delta, and Kappa). *J. Neurosci.* **1985**, *5* (3), 584−588.

(10) Mansour, A.; Khachaturian, H.; Lewis, M. E.; Akil, H.; Watson, S. J. Autoradiographic Differentiation of Mu, Delta, and Kappa Opioid Receptors in the Rat Forebrain and Midbrain. *J. Neurosci.* **1987**, *7* (8), 2445−2464.

(11) Lansu, K.; Karpiak, J.; Liu, J.; Huang, X.-P.; McCorvy, J. D.; Kroeze, W. K.; Che, T.; Nagase, H.; Carroll, F. I.; Jin, J.; Shoichet, B. K.; Roth, B. L. In Silico Design of Novel Probes for the Atypical Opioid Receptor MRGPRX2. *Nat. Chem. Biol.* **2017**, *13* (5), 529−536.

(12) Wacker, D.; Stevens, R. C.; Roth, B. L. How Ligands Illuminate GPCR Molecular Pharmacology. *Cell* **2017**, *170* (3), 414−427.

(13) Che, T.; Roth, B. L. Molecular Basis of Opioid Receptor Signaling. *Cell* **2023**, *186* (24), 5203−5219.

(14) Bohn, L. M.; Gainetdinov, R. R.; Lin, F.-T.; Lefkowitz, R. J.; Caron, M. G. μ-Opioid Receptor Desensitization by β-Arrestin-2 Determines Morphine Tolerance but Not Dependence. *Nature* **2000**, *408* (6813), 720−723.

(15) Bohn, L. M.; Lefkowitz, R. J.; Gainetdinov, R. R.; Peppel, K.; Caron, M. G.; Lin, F.-T. Enhanced Morphine Analgesia in Mice Lacking β-Arrestin 2. *Science* **1999**, *286* (5449), 2495−2498.

(16) Raehal, K. M.; Walker, J. K. L.; Bohn, L. M. Morphine Side Effects in β-Arrestin 2 Knockout Mice. *J. Pharmacol. Exp. Ther.* **2005**, *314* (3), 1195−1201.

(17) Schmid, C. L.; Kennedy, N. M.; Ross, N. C.; Lovell, K. M.; Yue, Z.; Morgenweck, J.; Cameron, M. D.; Bannister, T. D.; Bohn, L. M. Bias Factor and Therapeutic Window Correlate to Predict Safer Opioid Analgesics. *Cell* **2017**, *171* (5), 1165−1175.e13.
(18) DeWire, S. M.; Yamashita, D. S.; Rominger, D. H.; Liu, G.; Cowan, C. L.; Graczyk, T. M.; Chen, X.-T.; Pitis, P. M.; Gotchev, D.; Yuan, C.; Koblish, M.; Lark, M. W.; Violin, J. D. A G Protein-Biased Ligand at the μ-Opioid Receptor Is Potently Analgesic with Reduced Gastrointestinal and Respiratory Dysfunction Compared with Morphine. *J. Pharmacol. Exp. Ther.* **2013**, *344* (3), 708−717.
(19) Manglik, A.; Lin, H.; Aryal, D. K.; McCorvy, J. D.; Dengler, D.; Corder, G.; Levit, A.; Kling, R. C.; Bernat, V.; Hübner, H.; Huang, X.-P.; Sassano, M. F.; Giguère, P. M.; Löber, S.; Duan, D.; Scherrer, G.; Kobilka, B. K.; Gmeiner, P.; Roth, B. L.; Shoichet, B. K. Structure-Based Discovery of Opioid Analgesics with Reduced Side Effects. *Nature* **2016**, *537* (7619), 185−190.
(20) Wang, H.; Hetzer, F.; Huang, W.; Qu, Q.; Meyerowitz, J.; Kaindl, J.; Hübner, H.; Skiniotis, G.; Kobilka, B. K.; Gmeiner, P. Structure-Based Evolution of G Protein-Biased M-Opioid Receptor Agonists. *Angew. Chem., Int. Ed.* **2022**, *61* (26), No. e202200269.
(21) Qu, Q.; Huang, W.; Aydin, D.; Paggi, J. M.; Seven, A. B.; Wang, H.; Chakraborty, S.; Che, T.; DiBerto, J. F.; Robertson, M. J.; Inoue, A.; Suomivuori, C.-M.; Roth, B. L.; Majumdar, S.; Dror, R. O.; Kobilka, B. K.; Skiniotis, G. Insights into Distinct Signaling Profiles of the MOR Activated by Diverse Agonists. *Nat. Chem. Biol.* **2023**, *19* (4), 423−430.
(22) Levitt, E. S.; Abdala, A. P.; Paton, J. F. R.; Bissonnette, J. M.; Williams, J. T. μ Opioid Receptor Activation Hyperpolarizes Respiratory-controlling Kölliker−Fuse Neurons and Suppresses Post-inspiratory Drive. *J. Physiol.* **2015**, *593* (19), 4453−4469.
(23) Montandon, G.; Ren, J.; Victoria, N. C.; Liu, H.; Wickman, K.; Greer, J. J.; Horner, R. L. G-Protein−Gated Inwardly Rectifying Potassium Channels Modulate Respiratory Depression by Opioids. *Anesthesiology* **2016**, *124* (3), 641−650.
(24) Kliewer, A.; Schmiedel, F.; Sianati, S.; Bailey, A.; Bateman, J. T.; Levitt, E. S.; Williams, J. T.; Christie, M. J.; Schulz, S. Phosphorylation-Deficient G-Protein-Biased μ-Opioid Receptors Improve Analgesia and Diminish Tolerance but Worsen Opioid Side Effects. *Nat. Commun.* **2019**, *10* (1), No. 367.
(25) Kliewer, A.; Gillis, A.; Hill, R.; Schmiedel, F.; Bailey, C.; Kelly, E.; Henderson, G.; Christie, M. J.; Schulz, S. Morphine-induced Respiratory Depression Is Independent of B-arrestin2 Signalling. *Br. J. Pharmacol.* **2020**, *177* (13), 2923−2931.
(26) Yudin, Y.; Rohacs, T. The G-protein-biased Agents PZM21 and TRV130 Are Partial Agonists of M-opioid Receptor-mediated Signalling to Ion Channels. *Br. J. Pharmacol.* **2019**, *176* (17), 3110−3125.
(27) Gillis, A.; Gondin, A. B.; Kliewer, A.; Sanchez, J.; Lim, H. D.; Alamein, C.; Manandhar, P.; Santiago, M.; Fritzwanker, S.; Schmiedel, F.; Katte, T. A.; Reekie, T.; Grimsey, N. L.; Kassiou, M.; Kellam, B.; Krasel, C.; Halls, M. L.; Connor, M.; Lane, J. R.; Schulz, S.; Christie, M. J.; Canals, M. Low Intrinsic Efficacy for G Protein Activation Can Explain the Improved Side Effect Profiles of New Opioid Agonists. *Sci. Signaling* **2020**, *13* (625), No. eaaz3140.
(28) Tan, H. S.; Habib, A. S. Oliceridine: A Novel Drug for the Management of Moderate to Severe Acute Pain—A Review of Current Evidence. *J. Pain Res.* **2021**, *14*, 969−979.
(29) Conibear, A. E.; Kelly, E. A Biased View of μ-Opioid Receptors? *Mol. Pharmacol.* **2019**, *96* (5), 542−549.
(30) Aggarwal, A. K. Emerging Field of Biased Opioid Agonists. *Anesthesiol. Clin.* **2023**, *41* (2), 317−328.
(31) Tsai, M.-H. M.; Chen, L.; Baumann, M. H.; Canals, M.; Javitch, J. A.; Lane, J. R.; Shi, L. In Vitro Functional Profiling of Fentanyl and Nitazene Analogs at the μ-Opioid Receptor Reveals High Efficacy for Gi Protein Signaling. *ACS Chem. Neurosci.* **2024**, *15* (4), 854−867.
(32) Kelly, E.; Conibear, A.; Henderson, G. Biased Agonism: Lessons from Studies of Opioid Receptor Agonists. *Annu. Rev. Pharmacol. Toxicol.* **2023**, *63* (1), 491−515.
(33) Conibear, A.; Bailey, C. P.; Kelly, E. Biased Signalling in Analgesic Research and Development. *Curr. Opin. Pharmacol.* **2024**, *76*, No. 102465.
(34) Dahan, A.; Yassen, A.; Romberg, R.; Sarton, E.; Teppema, L.; Olofsen, E.; Danhof, M. Buprenorphine Induces Ceiling in Respiratory Depression but Not in Analgesia. *Br. J. Anaesth.* **2006**, *96* (5), 627−632.
(35) Wesson, D. R.; Smith, D. E. Buprenorphine in the Treatment of Opiate Dependence. *J. Psychoact. Drugs* **2010**, *42* (2), 161−175.
(36) Aiyer, R.; Gulati, A.; Gungor, S.; Bhatia, A.; Mehta, N. Treatment of Chronic Pain With Various Buprenorphine Formulations: A Systematic Review of Clinical Studies. *Anesth. Analg.* **2018**, *127* (2), 529−538.
(37) Shulman, M.; Wai, J. M.; Nunes, E. V. Buprenorphine Treatment for Opioid Use Disorder: An Overview. *CNS Drugs* **2019**, *33* (6), 567−580.
(38) Syal, S.; Ipser, J.; Terburg, D.; Solms, M.; Panksepp, J.; Malcolm-Smith, S.; Bos, P. A.; Montoya, E. R.; Stein, D. J.; van Honk, J. Improved Memory for Reward Cues Following Acute Buprenorphine Administration in Humans. *Psychoneuroendocrinology* **2015**, *53*, 10−15.
(39) Zubieta, J. Buprenorphine-Induced Changes in Mu-Opioid Receptor Availability in Male Heroin-Dependent Volunteers A Preliminary Study. *Neuropsychopharmacology* **2000**, *23* (3), 326−334.
(40) Gudin, J.; Fudin, J. A Narrative Pharmacological Review of Buprenorphine: A Unique Opioid for the Treatment of Chronic Pain. *Pain Ther.* **2020**, *9* (1), 41−54.
(41) Li, A. H.; Schmiesing, C.; Aggarwal, A. K. Evidence for Continuing Buprenorphine in the Perioperative Period. *Clin J. Pain* **2020**, *36* (10), 764−774.
(42) Pedersen, M. F.; Wróbel, T. M.; Märcher-Rørsted, E.; Pedersen, D. S.; Møller, T. C.; Gabriele, F.; Pedersen, H.; Matosiuk, D.; Foster, S. R.; Bouvier, M.; Bräuner-Osborne, H. Biased Agonism of Clinically Approved μ-Opioid Receptor Agonists and TRV130 Is Not Controlled by Binding and Signaling Kinetics. *Neuropharmacology* **2020**, *166*, No. 107718.
(43) Cong, X.; Maurel, D.; Déméné, H.; Vasiliauskaité-Brooks, I.; Hagelberger, J.; Peysson, F.; Saint-Paul, J.; Golebiowski, J.; Granier, S.; Sounier, R. Molecular Insights into the Biased Signaling Mechanism of the μ-Opioid Receptor. *Mol. Cell* **2021**, *81* (20), 4165−4175.e6.
(44) Uprety, R.; Che, T.; Zaidi, S. A.; Grinnell, S. G.; Varga, B. R.; Faouzi, A.; Slocum, S. T.; Allaoa, A.; Varadi, A.; Nelson, M.; Bernhard, S. M.; Kulko, E.; Le Rouzic, V.; Eans, S. O.; Simons, C. A.; Hunkele, A.; Subrath, J.; Pan, Y. X.; Javitch, J. A.; McLaughlin, J. P.; Roth, B. L.; Pasternak, G. W.; Katritch, V.; Majumdar, S. Controlling Opioid Receptor Functional Selectivity by Targeting Distinct Subpockets of the Orthosteric Site. *eLife* **2021**, *10*, No. e56519.
(45) Manglik, A.; Kruse, A. C.; Kobilka, T. S.; Thian, F. S.; Mathiesen, J. M.; Sunahara, R. K.; Pardo, L.; Weis, W. I.; Kobilka, B. K.; Granier, S. Crystal Structure of the M-Opioid Receptor Bound to a Morphinan Antagonist. *Nature* **2012**, *485* (7398), 321−326.
(46) Zhuang, Y.; Wang, Y.; He, B.; He, X.; Zhou, X. E.; Guo, S.; Rao, Q.; Yang, J.; Liu, J.; Zhou, Q.; Wang, X.; Liu, M.; Liu, W.; Jiang, X.; Yang, D.; Jiang, H.; Shen, J.; Melcher, K.; Chen, H.; Jiang, Y.; Cheng, X.; Wang, M.-W.; Xie, X.; Xu, H. E. Molecular Recognition of Morphine and Fentanyl by the Human μ-Opioid Receptor. *Cell* **2022**, *185* (23), 4361−4375.e19.
(47) Huang, W.; Manglik, A.; Venkatakrishnan, A. J.; Laeremans, T.; Feinberg, E. N.; Sanborn, A. L.; Kato, H. E.; Livingston, K. E.; Thorsen, T. S.; Kling, R. C.; Granier, S.; Gmeiner, P.; Husbands, S. M.; Traynor, J. R.; Weis, W. I.; Steyaert, J.; Dror, R. O.; Kobilka, B. K. Structural Insights into M-Opioid Receptor Activation. *Nature* **2015**, *524* (7565), 315−321.
(48) O'Brien, E. S.; Rangari, V. A.; El Daibani, A.; Eans, S. O.; Hammond, H. R.; White, E.; Wang, H.; Shiimura, Y.; Kumar, K. K.; Jiang, Q.; Appourchaux, K.; Huang, W.; Zhang, C.; Kennedy, B. J.; Mathiesen, J. M.; Che, T.; McLaughlin, J. P.; Majumdar, S.; Kobilka,

https://doi.org/10.1021/acs.jcim.5c00078
J. Chem. Inf. Model. 2025, 65, 5071−5085

B. K. A M-Opioid Receptor Modulator That Works Cooperatively with Naloxone. *Nature* **2024**, *631* (8021), 686−693.
(49) Sounier, R.; Mas, C.; Steyaert, J.; Laeremans, T.; Manglik, A.; Huang, W.; Kobilka, B. K.; Déméné, H.; Granier, S. Propagation of Conformational Changes during μ-Opioid Receptor Activation. *Nature* **2015**, *524* (7565), 375−378.
(50) Sutcliffe, K. J.; Henderson, G.; Kelly, E.; Sessions, R. B. Drug Binding Poses Relate Structure with Efficacy in the μ Opioid Receptor. *J. Mol. Biol.* **2017**, *429* (12), 1840−1851.
(51) Kelly, B.; Hollingsworth, S. A.; Blakemore, D. C.; Owen, R. M.; Storer, R. I.; Swain, N. A.; Aydin, D.; Torella, R.; Warmus, J. S.; Dror, R. O. Delineating the Ligand−Receptor Interactions That Lead to Biased Signaling at the μ-Opioid Receptor. *J. Chem. Inf. Model.* **2021**, *61* (7), 3696−3707.
(52) Sena, D. M.; Cong, X.; Giorgetti, A. Ligand Based Conformational Space Studies of the μ-Opioid Receptor. *Biochim. Biophys. Acta, Gen. Subj.* **2021**, *1865* (3), No. 129838.
(53) Vo, Q. N.; Mahinthichaichan, P.; Shen, J.; Ellis, C. R. How μ-Opioid Receptor Recognizes Fentanyl. *Nat. Commun.* **2021**, *12* (1), No. 984.
(54) Bartuzi, D.; Kaczor, A. A.; Matosiuk, D. Molecular Mechanisms of Allosteric Probe Dependence in μ Opioid Receptor. *J. Biomol. Struct. Dyn.* **2019**, *37* (1), 36−47.
(55) Cheng, J.-x.; Cheng, T.; Li, W.; Liu, G.; Zhu, W.; Tang, Y. Computational Insights into the G-Protein-Biased Activation and Inactivation Mechanisms of the μ Opioid Receptor. *Acta Pharmacol. Sin.* **2018**, *39* (1), 154−164.
(56) Ricarte, A.; Dalton, J. A. R.; Giraldo, J. Structural Assessment of Agonist Efficacy in the μ-Opioid Receptor: Morphine and Fentanyl Elicit Different Activation Patterns. *J. Chem. Inf. Model.* **2021**, *61* (3), 1251−1274.
(57) Xie, B.; Goldberg, A.; Shi, L. A Comprehensive Evaluation of the Potential Binding Poses of Fentanyl and Its Analogs at the M-Opioid Receptor. *Comput. Struct. Biotechnol. J.* **2022**, *20*, 2309−2321.
(58) Provasi, D.; Bortolato, A.; Filizola, M. Exploring Molecular Mechanisms of Ligand Recognition by Opioid Receptors with Metadynamics. *Biochemistry* **2009**, *48* (42), 10020−10029.
(59) Schneider, S.; Provasi, D.; Filizola, M. How Oliceridine (TRV-130) Binds and Stabilizes a μ-Opioid Receptor Conformational State That Selectively Triggers G Protein Signaling Pathways. *Biochemistry* **2016**, *55* (46), 6456−6466.
(60) Kapoor, A.; Martinez-Rosell, G.; Provasi, D.; de Fabritiis, G.; Filizola, M. Dynamic and Kinetic Elements of M-Opioid Receptor Functional Selectivity. *Sci. Rep.* **2017**, *7* (1), No. 11255.
(61) Ribeiro, J. M. L.; Provasi, D.; Filizola, M. A Combination of Machine Learning and Infrequent Metadynamics to Efficiently Predict Kinetic Rates, Transition States, and Molecular Determinants of Drug Dissociation from G Protein-Coupled Receptors. *J. Chem. Phys.* **2020**, *153* (12), No. 124105.
(62) Saleh, N.; Ibrahim, P.; Saladino, G.; Gervasio, F. L.; Clark, T. An Efficient Metadynamics-Based Protocol To Model the Binding Affinity and the Transition State Ensemble of G-Protein-Coupled Receptor Ligands. *J. Chem. Inf. Model.* **2017**, *57* (5), 1210−1217.
(63) Ballesteros, J. A.; Weinstein, H.[19] Integrated Methods for the Construction of Three-Dimensional Models and Computational Probing of Structure-Function Relations in G Protein-Coupled Receptors. In *Methods in Neurosciences*; Elsevier, 1995; Vol. *25*, pp 366−428.
(64) Santos-Martins, D.; Solis-Vasquez, L.; Tillack, A. F.; Sanner, M. F.; Koch, A.; Forli, S. Accelerating AutoDock4 with GPUs and Gradient-Based Local Search. *J. Chem. Theory Comput.* **2021**, *17* (2), 1060−1073.
(65) Robertson, M. J.; Papasergi-Scott, M. M.; He, F.; Seven, A. B.; Meyerowitz, J. G.; Panova, O.; Peroto, M. C.; Che, T.; Skiniotis, G. Structure Determination of Inactive-State GPCRs with a Universal Nanobody. *Nat. Struct. Mol. Biol.* **2022**, *29* (12), 1188−1195.
(66) Volpe, D. A.; Tobin, G. A. M.; Mellon, R. D.; Katki, A. G.; Parker, R. J.; Colatsky, T.; Kropp, T. J.; Verbois, S. L. Uniform Assessment and Ranking of Opioid Mu Receptor Binding Constants for Selected Opioid Drugs. *Regul. Toxicol. Pharmacol.* **2011**, *59* (3), 385−390.
(67) Ben Haddou, T.; Béni, S.; Hosztafi, S.; Malfacini, D.; Calo, G.; Schmidhammer, H.; Spetea, M. Pharmacological Investigations of N-Substituent Variation in Morphine and Oxymorphone: Opioid Receptor Binding, Signaling and Antinociceptive Activity. *PLoS One* **2014**, *9* (6), No. e99231.
(68) Pillarisetti, S.; Khanna, I. Buprenorphine—an Attractive Opioid with Underutilized Potential in Treatment of Chronic Pain. *J. Pain Res.* **2015**, 859−870.
(69) Koehl, A.; Hu, H.; Maeda, S.; Zhang, Y.; Qu, Q.; Paggi, J. M.; Latorraca, N. R.; Hilger, D.; Dawson, R.; Matile, H.; Schertler, G. F. X.; Granier, S.; Weis, W. I.; Dror, R. O.; Manglik, A.; Skiniotis, G.; Kobilka, B. K. Structure of the M-Opioid Receptor−Gi Protein Complex. *Nature* **2018**, *558* (7711), 547−552.
(70) Weis, W. I.; Kobilka, B. K. The Molecular Basis of G Protein−Coupled Receptor Activation. *Annu. Rev. Biochem.* **2018**, *87* (1), 897−919.
(71) Laurent, B.; Chavent, M.; Cragnolini, T.; Dahl, A. C. E.; Pasquali, S.; Derreumaux, P.; Sansom, M. S. P.; Baaden, M. Epock: Rapid Analysis of Protein Pocket Dynamics. *Bioinformatics* **2015**, *31* (9), 1478−1480.
(72) Zhao, J.; Elgeti, M.; O'Brien, E. S.; Sár, C. P.; EI Daibani, A.; Heng, J.; Sun, X.; White, E.; Che, T.; Hubbell, W. L.; Kobilka, B. K.; Chen, C. Ligand Efficacy Modulates Conformational Dynamics of the M-Opioid Receptor. *Nature* **2024**, *629* (8011), 474−480.
(73) Granier, S.; Manglik, A.; Kruse, A. C.; Kobilka, T. S.; Thian, F. S.; Weis, W. I.; Kobilka, B. K. Structure of the δ-Opioid Receptor Bound to Naltrindole. *Nature* **2012**, *485* (7398), 400−404.
(74) Fenalti, G.; Zatsepin, N. A.; Betti, C.; Giguere, P.; Han, G. W.; Ishchenko, A.; Liu, W.; Guillemyn, K.; Zhang, H.; James, D.; Wang, D.; Weierstall, U.; Spence, J. C. H.; Boutet, S.; Messerschmidt, M.; Williams, G. J.; Gati, C.; Yefanov, O. M.; White, T. A.; Oberthuer, D.; Metz, M.; Yoon, C. H.; Barty, A.; Chapman, H. N.; Basu, S.; Coe, J.; Conrad, C. E.; Fromme, R.; Fromme, P.; Tourwé, D.; Schiller, P. W.; Roth, B. L.; Ballet, S.; Katritch, V.; Stevens, R. C.; Cherezov, V. Structural Basis for Bifunctional Peptide Recognition at Human δ-Opioid Receptor. *Nat. Struct. Mol. Biol.* **2015**, *22* (3), 265−268.
(75) El Daibani, A.; Paggi, J. M.; Kim, K.; Laloudakis, Y. D.; Popov, P.; Bernhard, S. M.; Krumm, B. E.; Olsen, R. H. J.; Diberto, J.; Carroll, F. I.; Katritch, V.; Wünsch, B.; Dror, R. O.; Che, T. Molecular Mechanism of Biased Signaling at the Kappa Opioid Receptor. *Nat. Commun.* **2023**, *14* (1), No. 1338.
(76) Cami-Kobeci, G.; Polgar, W. E.; Khroyan, T. V.; Toll, L.; Husbands, S. M. Structural Determinants of Opioid and NOP Receptor Activity in Derivatives of Buprenorphine. *J. Med. Chem.* **2011**, *54* (19), 6531−6537.
(77) Miyazaki, T.; Choi, I. Y.; Rubas, W.; Anand, N. K.; Ali, C.; Evans, J.; Gursahani, H.; Hennessy, M.; Kim, G.; McWeeney, D.; Pfeiffer, J.; Quach, P.; Gauvin, D.; Riley, T. A.; Riggs, J. A.; Gogas, K.; Zalevsky, J.; Doberstein, S. K. NKTR-181: A Novel Mu-Opioid Analgesic with Inherently Low Abuse Potential. *J. Pharmacol. Exp. Ther.* **2017**, *363* (1), 104−113.
(78) Verteramo, M. L.; Stenström, O.; Ignjatović, M. M.; Caldararu, O.; Olsson, M. A.; Manzoni, F.; Leffler, H.; Oksanen, E.; Logan, D. T.; Nilsson, U. J.; Ryde, U.; Akke, M. Interplay between Conformational Entropy and Solvation Entropy in Protein−Ligand Binding. *J. Am. Chem. Soc.* **2019**, *141* (5), 2012−2026.
(79) Chavkin, C.; Goldstein, A. Specific Receptor for the Opioid Peptide Dynorphin: Structure–Activity Relationships. *Proc. Natl. Acad. Sci. U.S.A.* **1981**, *78* (10), 6543−6547.
(80) Pasternak, G. W.; Pan, Y.-X.; Sibley, D. R. Mu Opioids and Their Receptors: Evolution of a Concept. *Pharmacol. Rev.* **2013**, *65* (4), 1257−1317.
(81) Spetea, M.; Schmidhammer, H. Opioids and Their Receptors: Present and Emerging Concepts in Opioid Drug Discovery. *Molecules* **2020**, *25* (23), No. 5658.

https://doi.org/10.1021/acs.jcim.5c00078
J. Chem. Inf. Model. 2025, 65, 5071−5085

(82) Shi, L.; Liapakis, G.; Xu, R.; Guarnieri, F.; Ballesteros, J. A.; Javitch, J. A. B2 Adrenergic Receptor Activation. *J. Biol. Chem.* **2002**, *277* (43), 40989−40996.
(83) Holst, B.; Nygaard, R.; Valentin-Hansen, L.; Bach, A.; Engelstoft, M. S.; Petersen, P. S.; Frimurer, T. M.; Schwartz, T. W. A Conserved Aromatic Lock for the Tryptophan Rotameric Switch in TM-VI of Seven-Transmembrane Receptors. *J. Biol. Chem.* **2010**, *285* (6), 3973−3985.
(84) Xu, H.; Lu, Y. F.; Partilla, J. S.; Zheng, Q. X.; Wang, J. B.; Brine, G. A.; Carroll, F. I.; Rice, K. C.; Chen, K. X.; Chi, Z. Q.; Rothman, R. B. Opioid Peptide Receptor Studies, 11: Involvement of Tyr148, Trp318 and His319 of the Rat Mu-Opioid Receptor in Binding of Mu-Selective Ligands. *Synapse* **1999**, *32* (1), 23−28.
(85) Huang, P.; Kehner, G. B.; Cowan, A.; Liu-Chen, L.-Y. Comparison of Pharmacological Activities of Buprenorphine and Norbuprenorphine: Norbuprenorphine Is a Potent Opioid Agonist. *J. Pharmacol. Exp. Ther.* **2001**, *297* (2), 688−695.
(86) Li, G.; Aschenbach, L. C.; Chen, J.; Cassidy, M. P.; Stevens, D. L.; Gabra, B. H.; Selley, D. E.; Dewey, W. L.; Westkaemper, R. B.; Zhang, Y. Design, Synthesis, and Biological Evaluation of 6α- and 6β-*N* -Heterocyclic Substituted Naltrexamine Derivatives as μ Opioid Receptor Selective Antagonists. *J. Med. Chem.* **2009**, *52* (5), 1416−1427.
(87) Deupi, X.; Li, X.-D.; Schertler, G. F. X. Ligands Stabilize Specific GPCR Conformations: But How? *Structure* **2012**, *20* (8), 1289−1290.
(88) Heydenreich, F. M.; Marti-Solano, M.; Sandhu, M.; Kobilka, B. K.; Bouvier, M.; Babu, M. M. Molecular Determinants of Ligand Efficacy and Potency in GPCR Signaling. *Science* **2023**, *382* (6677), No. eadh1859.
(89) Polacco, B. J.; Lobingier, B. T.; Blythe, E. E.; Abreu, N.; Khare, P.; Howard, M. K.; Gonzalez-Hernandez, A. J.; Xu, J.; Li, Q.; Novy, B.; Naing, Z. Z. C.; Shoichet, B. K.; Coyote-Maestas, W.; Levitz, J.; Krogan, N. J.; Von Zastrow, M.; Hüttenhain, R. Profiling the Proximal Proteome of the Activated μ-Opioid Receptor. *Nat. Chem. Biol.* **2024**, *20* (9), 1133−1143.
(90) Leff, P.; Scaramellini, C.; Law, C.; McKechnie, K. A Three-State Receptor Model of Agonist Action. *Trends Pharmacol. Sci.* **1997**, *18* (10), 355−362.
(91) Waterhouse, A.; Bertoni, M.; Bienert, S.; Studer, G.; Tauriello, G.; Gumienny, R.; Heer, F. T.; de Beer, T. A. P.; Rempfer, C.; Bordoli, L.; Lepore, R.; Schwede, T. SWISS-MODEL: Homology Modelling of Protein Structures and Complexes. *Nucleic Acids Res.* **2018**, *46* (W1), W296−W303.
(92) Olsson, M. H. M.; Søndergaard, C. R.; Rostkowski, M.; Jensen, J. H. PROPKA3: Consistent Treatment of Internal and Surface Residues in Empirical p K_a Predictions. *J. Chem. Theory Comput.* **2011**, *7* (2), 525−537.
(93) Kim, S.; Lee, J.; Jo, S.; Brooks, C. L.; Lee, H. S.; Im, W. CHARMM-GUI Ligand Reader and Modeler for CHARMM Force Field Generation of Small Molecules. *J. Comput. Chem.* **2017**, *38* (21), 1879−1886.
(94) Morris, G. M.; Huey, R.; Lindstrom, W.; Sanner, M. F.; Belew, R. K.; Goodsell, D. S.; Olson, A. J. AutoDock4 and AutoDockTools4: Automated Docking with Selective Receptor Flexibility. *J. Comput. Chem.* **2009**, *30* (16), 2785−2791.
(95) Jo, S.; Lim, J. B.; Klauda, J. B.; Im, W. CHARMM-GUI Membrane Builder for Mixed Bilayers and Its Application to Yeast Membranes. *Biophys. J.* **2009**, *97* (1), 50−58.
(96) Vanommeslaeghe, K.; Hatcher, E.; Acharya, C.; Kundu, S.; Zhong, S.; Shim, J.; Darian, E.; Guvench, O.; Lopes, P.; Vorobyov, I.; Mackerell, A. D. CHARMM General Force Field: A Force Field for Drug-like Molecules Compatible with the CHARMM All-atom Additive Biological Force Fields. *J. Comput. Chem.* **2010**, *31* (4), 671−690.
(97) Abraham, M. J.; Murtola, T.; Schulz, R.; Páll, S.; Smith, J. C.; Hess, B.; Lindahl, E. GROMACS: High Performance Molecular Simulations through Multi-Level Parallelism from Laptops to Supercomputers. *SoftwareX* **2015**, *1*−*2*, 19−25.
(98) Huang, J.; Rauscher, S.; Nawrocki, G.; Ran, T.; Feig, M.; de Groot, B. L.; Grubmüller, H.; MacKerell, A. D. CHARMM36m: An Improved Force Field for Folded and Intrinsically Disordered Proteins. *Nat. Methods* **2017**, *14* (1), 71−73.
(99) Bussi, G.; Donadio, D.; Parrinello, M. Canonical Sampling through Velocity Rescaling. *J. Chem. Phys.* **2007**, *126* (1), No. 014101.
(100) Parrinello, M.; Rahman, A. Polymorphic Transitions in Single Crystals: A New Molecular Dynamics Method. *J. Appl. Phys.* **1981**, *52* (12), 7182−7190.
(101) Essmann, U.; Perera, L.; Berkowitz, M. L.; Darden, T.; Lee, H.; Pedersen, L. G. A Smooth Particle Mesh Ewald Method. *J. Chem. Phys.* **1995**, *103* (19), 8577−8593.
(102) Tribello, G. A.; Bonomi, M.; Branduardi, D.; Camilloni, C.; Bussi, G. PLUMED 2: New Feathers for an Old Bird. *Comput. Phys. Commun.* **2014**, *185* (2), 604−613.
(103) Laio, A.; Parrinello, M. Escaping Free-Energy Minima. *Proc. Natl. Acad. Sci. U.S.A.* **2002**, *99* (20), 12562−12566.
(104) Barducci, A.; Bussi, G.; Parrinello, M. Well-Tempered Metadynamics: A Smoothly Converging and Tunable Free-Energy Method. *Phys. Rev. Lett.* **2008**, *100* (2), No. 020603.
(105) Mattedi, G.; Deflorian, F.; Mason, J. S.; de Graaf, C.; Gervasio, F. L. Understanding Ligand Binding Selectivity in a Prototypical GPCR Family. *J. Chem. Inf. Model.* **2019**, *59* (6), 2830−2836.
(106) Söldner, C. A.; Horn, A. H. C.; Sticht, H. Binding of Histamine to the H1 Receptor—a Molecular Dynamics Study. *J. Mol. Model.* **2018**, *24* (12), No. 346.
(107) Raiteri, P.; Laio, A.; Gervasio, F. L.; Micheletti, C.; Parrinello, M. Efficient Reconstruction of Complex Free Energy Landscapes by Multiple Walkers Metadynamics. *J. Phys. Chem. B* **2006**, *110* (8), 3533−3539.
(108) Limongelli, V.; Bonomi, M.; Parrinello, M. Funnel Metadynamics as Accurate Binding Free-Energy Method. *Proc. Natl. Acad. Sci. U.S.A.* **2013**, *110* (16), 6358−6363.
(109) Humphrey, W.; Dalke, A.; Schulten, K. VMD: Visual Molecular Dynamics. *J. Mol. Graphics* **1996**, *14* (1), 33−38.
(110) Steiner, T. The Hydrogen Bond in the Solid State. *Angew. Chem., Int. Ed.* **2002**, *41* (1), 49−76.

https://doi.org/10.1021/acs.jcim.5c00078
J. Chem. Inf. Model. 2025, 65, 5071−5085